Marine Geology 411 (2019) 36–50

Contents lists available at ScienceDirect

Marine Geology

journal homepage: www.elsevier.com/locate/margo

Review article

New K/Ar age values and context from published clay mineralogy and Sr and Nd isotopes as tracers of terrigenous Atlantic Ocean sediments

Sidney R. Hemming

Department of Earth and Environmental Sciences and Lamont-Doherty Earth Observatory of Columbia University, 61 Rt. 9W, Palisades, NY 10964

ARTICLE INFO

Editor: G.J. de Lange

Keywords:
Radiogenic isotopes
Strontium isotopes
Neodymium isotopes
Provenance
Clay minerals

ABSTRACT

Sediment particles derived from the continents have compositional variability that allows them to be used as tracers from their sources. Because of the patchwork of geological terrains that make up the continents, radiogenic isotope daughters of long-half-life parents provide a powerful tool for understanding the origins and dispersal patterns of sediments. Weathering processes that prevail in different climatic zones further imprint the geochemical signature of sources. Fine-grained sediments, clays and silts, can travel long distances in winds and ocean currents, and changes in their composition through time may allow understanding changes in their transporting media and climate significance. This paper presents new K/Ar age values of fine sediments in the Atlantic Ocean basin. The paper also presents a brief overview of the important factors of sediment delivery to the Atlantic Ocean, and reviews the new K/Ar data within the context of published clay mineralogy and $^{87}Sr/^{86}Sr$ from the same samples. Additionally, the paper presents previously published K/Ar and $^{87}Sr/^{86}Sr$ and ε_{Nd} from Atlantic Ocean sediments, and uses the map distributions as a way to qualitatively compare the compositional trends of the four tracers as many of the data are from different samples. Although the information for all of these provenance tracers is incomplete and it would be fruitful to fill in many different aspects, this compilation of previously published K/Ar, $^{87}Sr/^{86}Sr$ and ε_{Nd} data compared with the new data demonstrates that the distribution of K/Ar ages is broadly consistent with the other compositional information and with the geology of the surrounding continents. K/Ar provenance ages offer a simple and reliable tracer of sediment sources that is complementary to other methods.

1. Introduction

The compositions of terrigenous marine sediments provide important constraints on the processes that brought them to their depositional sites in the ocean. The mineralogical content and geochemical composition of sediments reflect the source rock types, weathering style and intensity, as well as sedimentary sorting (e.g., Taylor and McLennan, 1985), and thus measurements of these parameters elucidate the integrated provenance and processes that have acted on the sediments and their sources. Radiogenic isotopes provide a measure of the temporal geologic history of sediments that may be different depending on the geochemical characteristics of the parent and daughter isotopes and the geological histories of the sources that contribute to the mixtures (e.g., Aarons et al., 2013; Basile et al., 1997; Biscaye and Dasch, 1971; Clauer and Chaudhuri, 1995; Cole et al., 2009; Dasch, 1969; de Mahiques et al., 2008; DePaolo et al., 2006; Fagel et al., 1999, 2004; Fagel and Mattielli, 2011; Farmer et al., 2003; Franzese et al., 2006; Franzese et al., 2009; Franzese and Hemming, 2013; Goldstein and Jacobsen, 1988; Goldstein, 1988; Goldstein et al., 1984; Gombiner et al., 2016; Grousset et al., 2001, 1998, 1993, 1988; Grousset and Biscaye, 2005, 1989; Hegner et al., 2007; Hemming et al., 2002; Huon and Jantschik, 1993; Huon and Ruch, 1992; Hurley, 1961; Hurley et al., 1963b, 1961; Innocent et al., 2000, 1997; Jantschik and Huon, 1992; Jones et al., 1994; Kumar et al., 2014; McCulloch and Wasserburg, 1978; McLennan et al., 1990; Meyer et al., 2011; Nakai et al., 1993; Noble et al., 2012; Onions et al., 1983; Pettke et al., 2000; Revel et al., 1996; Reyes et al., 2014; Skonieczny et al., 2013; Toucanne et al., 2015; VanLaningham et al., 2009, 2008, 2006; VanLaningham and Mark, 2011; Walter et al., 2000). The K/Ar system in fine-grained terrigenous sediments tends to represent the latest stages of the geologic history of the sediments' sources because K-bearing minerals are susceptible to weathering and then are reconstituted during sedimentary diagenesis, and because they are also susceptible to argon loss during metamorphic mineral growth and thermal diffusion. The K/Ar bulk age value of fine-grained sediments has been found to be a useful measure of sediment provenance in a number of previous studies (Gombiner et al., 2016; Hemming et al., 2002; Huon and Ruch, 1992; Hurley et al., 1961, 1963b, 1963a; Jantschik and Huon, 1992; Pettke et al., 2000;

E-mail address: srh17@columbia.edu.

https://doi.org/10.1016/j.margeo.2019.01.007
Received 19 June 2018; Received in revised form 4 January 2019; Accepted 18 January 2019
Available online 07 February 2019

VanLaningham et al., 2006, 2008, 2009; VanLaningham and Mark, 2011), but it is still not as widely used as other isotopic methods.

These previous studies have demonstrated the promise of the K/Ar system for the study of terrigenous sediment provenance. Hurley's pioneering work from the early 1960's showed that modern river sediments give K/Ar ages that are greatly in excess of their depositional ages and are in general agreement with what is known about the geological history their sources (Hurley et al., 1961). Hurley (Hurley et al., 1963a) found that fine-grained Atlantic sediments between 0° and 29°N have K/Ar ages ranging from 85 to 460 Ma, and Hurley et al. (Hurley et al., 1963b) showed that ancient shales have K/Ar ages that range from near their depositional age to greatly in excess of their depositional age. Hurley et al. (Hurley et al., 1963b) interpreted the old ages found in fine sediments to be the result of a dominance of detrital dioctohedral mica (illite) in the modern sediments, and the ages approaching depositional ages in ancient sediments to be due to creation of new mica during diagenesis. Surface sediments in the so-call Ruddiman or IRD belt (Ruddiman, 1977) of the eastern North Atlantic have ages of approximately 400 Ma (Hemming et al., 2002; Jantschik and Huon, 1992).

After a gap following Hurley's work on sediment provenance with K/Ar, one of the first geochemical applications to the provenance of "Heinrich events" was the K/Ar system (Huon and Ruch, 1992; Jantschik and Huon, 1992). Heinrich events are layers in the North Atlantic IRD belt that contain high percentages of mineral or rock grains in the sand fractions (Heinrich, 1988) and that have evidence for massive discharges of icebergs into the North Atlantic (Bond et al., 1992; Broecker et al., 1992; Grousset et al., 1993; Hemming, 2004; McManus et al., 1998). Jantschik and Huon (1992) found that Heinrich events from the Dreizack Seamounts give K/Ar ages of approximately 1 Ga, in contrast to the ambient 400 Ma ages, and this is one of the key pieces of information pointing to a Canadian Shield source for Heinrich events. Hemming et al. (2002) followed up on the K/Ar observations with $^{40}Ar/^{39}Ar$ and $^{40}Ar^*$ measurements of North Atlantic sediments. They found that the stepped-release spectra for Heinrich layer sediments gave a relatively small range of ages, and they also found that the dominant signal of the K/Ar age is the concentration of $^{40}Ar^*$ The relatively small range in K concentrations, with average of approximately 2%, leaves age as the main variable controlling the concentration of $^{40}Ar^*$ in fine terrigenous sediments.

Several published studies from the Pacific basin highlight the value of the K/Ar system in fine-grained sediments. The center of the North Pacific has long been known to have terrigenous sediment compositions that contrast with the marginal sediments around the basin, and that derive from Asian dust deposition (Griffin et al., 1968; Jones et al., 1994; Nakai et al., 1993; Pettke et al., 2000; Rea et al., 1985). Pettke et al. (2000) used a variety of tracers, including $^{40}Ar/^{39}Ar$ to track the variations in provenance to the North Pacific over the past 12 million years. They found that although the fluxes and mineralogy varied, the $^{40}Ar/^{39}Ar$ age is ~200 Ma through the record and is consistent with other radiogenic provenance data that imply a constant source region from Asia supplying the sediment since at least 12 Ma.

In more marginal sites in the eastern Pacific (Gombiner et al., 2016; VanLaningham et al., 2008) and in the northwestern Pacific (VanLaningham et al., 2009), the K/Ar system has been paired with ε_{Nd} to understand the sources of sediment input near the margins. VanLaningham et al. (2008) used a combination of clay mineralogy, ε_{Nd} and $^{40}Ar/^{39}Ar$ to characterize the output from rivers from approximately 38° to 47° N along the North American- Pacific margin, and to examine a record through time from a sediment core. Mixing of reasonable proportions of modern rivers explains the Holocene results from the core, but an additional source that they attribute to increased input from glaciation in the Cascade Range, is required to explain the 25–20 ka deposits. These background data also provide important context for the goal of discerning the evidence for glacial outburst floods from Lake Missoula through the Columbia River. Gombiner et al. (2016) presented evidence of cyclic flood events from a core near Vancouver Island, with K/Ar ages that are too old to be explained by local sources and that can be used to constrain the provenance information from more widely available elemental analyses. There are at least 44 layers within that core that appear to have a source from the Missoula floods. Paired K/Ar ages and ε_{Nd} for sediments from Lake Missoula and from slackwater deposits along the scablands drainage provide further support for the interpreted provenance. In another example VanLaningham et al. (2009) used the combination of Nd isotopes and $^{40}Ar/^{39}Ar$ to examine provenance changes in a core on the Meiji Drift in the northwest Pacific Ocean, The Meiji Drift is thought to have originated from deposition in deepwater flow from the Bering Sea, and the data from glacial periods is significantly different from that of interglacial periods and is supportive of a Bearing Sea contribution in glacial periods. Interglacial sediments are well explained by more proximal Kamchatkan and Aleutian sources while older source rocks such as those found in the Yukon and northeastern Russia are major contributors during the glacial intervals, and the authors' mixing models suggest 35–35% of the sediment during glacial intervals is from the Bering Sea.

The applications of the K/Ar system reviewed above indicate that it may be a powerful provenance tool, but a first order question for any provenance tool is how the signal is integrated in the potential source catchments. Recent experimental results probe the application of the K/Ar system as provenance indicator in silt-size sediments. VanLaningham and Mark (2011) developed a particularly convincing case study in Alaska's Yukon River basin. First, using georeferenced K/Ar and Ar/Ar data from the USGS and NRCAN geochronological databases, they calculated the average crystallization/cooling age of rocks in the Yukon River catchment to be 121 Ma. This age represented the testable hypothesis of the experiment: The $^{40}Ar/^{39}Ar$ age of sediments from the Yukon River should match the average $^{40}Ar/^{39}Ar$ age of the sediment's source rocks - 121 Ma in this case. To test this hypothesis, they conducted step-heating experiments on both suspended load and bedload sediments from the Yukon River, in each case isolating the 20–63 um fraction to minimize the ^{39}Ar recoil effect on the apparent ages. They determined a plateau age of 115.4 ± 1.3 Ma for the suspended load sample and a plateau age of 119.6 ± 0.6 Ma for the bedload sample. The ages are a close match to the expected age of 121 Ma, confirming their hypothesis, and suggesting the broader truth that $^{40}Ar/^{39}Ar$ ages of fine-grained sediments reflect the integrated age of the sediment's source rocks.

Presented here are new K/Ar age values calculated from $^{40}Ar^*$ (that is, the ^{40}Ar that is radiogenic, determined by subtracting the atmospheric contribution using the measured ^{36}Ar) concentration data from a subset of 43 samples from the Biscaye (1965) Atlantic clay mineral survey (Fig. 1) to provide a comparison of K/Ar ages of the clay fractions (< 2 μm) from modern Atlantic Ocean sediments with previously published provenance data from clay mineralogy. I also compare the results with published $^{87}Sr/^{86}Sr$ and ε_{Nd} from terrigenous Atlantic sediments. K/Ar age values for a set of 12 Holocene and 14 glacial samples taken from cores along the mid-Atlantic ridge (MAR) are also presented. I conclude that the K/Ar system is a useful tool for understanding provenance, providing information that is complementary to other provenance tracers.

2. Background

2.1. Distribution of clay minerals in the Atlantic Ocean

Pierre Biscaye's Ph.D. thesis (Biscaye, 1965) on the distribution of clay minerals in the Atlantic Basin, as well as the global summary of clay mineral distributions (Griffin et al., 1968) revealed fundamental aspects of sediment provenance and weathering processes. Montmorillonite is found in low abundances throughout the Atlantic Basin, except near Antarctica where the abundance is much higher. Illite is

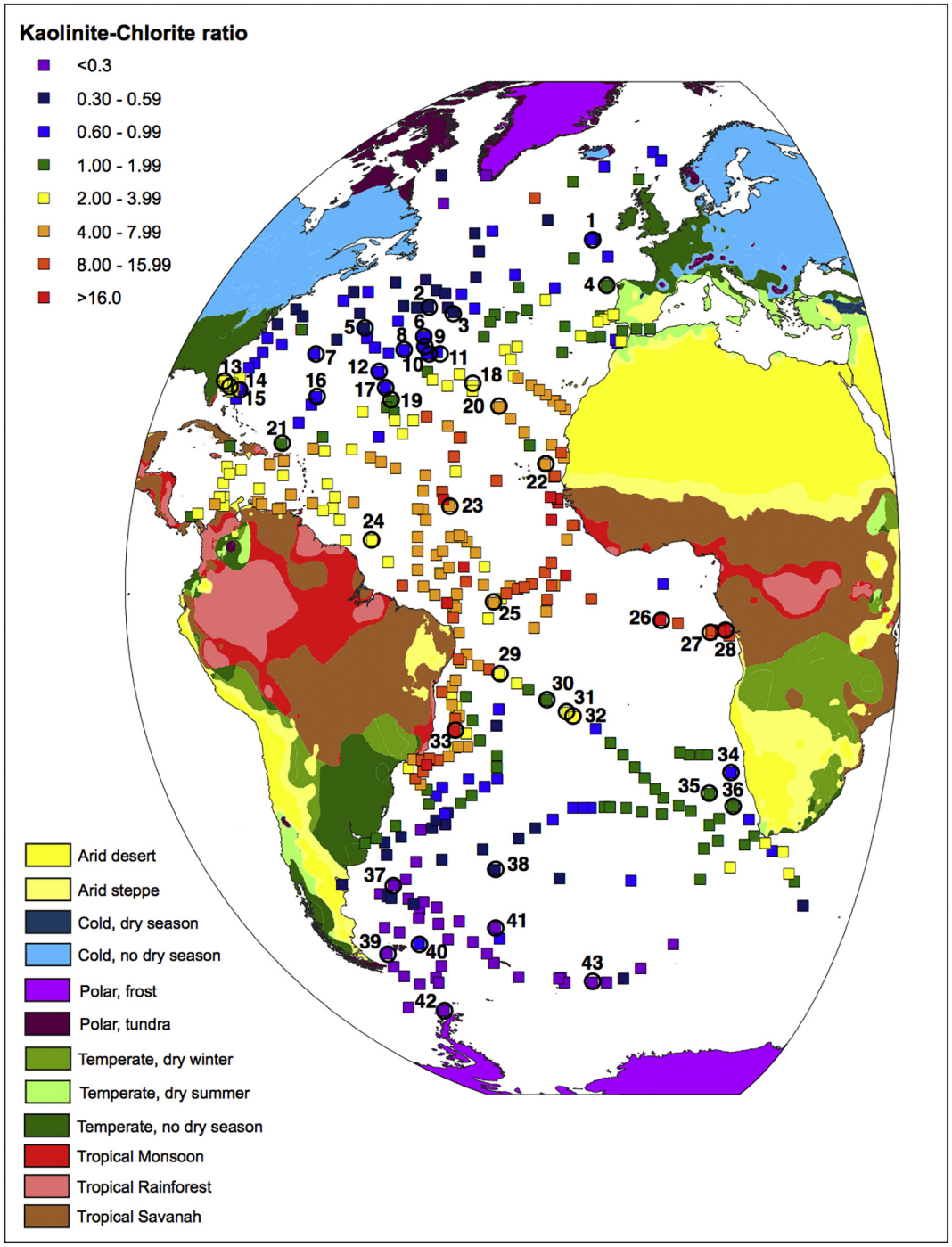

Fig. 1. Map of kaolinite to chlorite ratio of < 2 μm terrigenous, near-surface sediments in the Atlantic Ocean and climate zones on the surrounding continents. The clay data are archived at http://www.earthchem.org/library/browse/view?id=981 (Biscaye, 1965). The climate zones are from Peel et al. (2007). Samples for which ^{40}Ar*data are reported are numbered on the map as in in Table 2.

considered a purely detrital component and is found in high concentrations across the sub-polar North Atlantic, particularly on the eastern side, in a zone from Florida to North Africa, near the southern tips of South America and South Africa, and near the outlets of all the major rivers in South America. Chlorite concentrations are high in both the far North Atlantic/Nordic Seas (as well as near the gulf of St Lawrence) and far South Atlantic, and this distribution is attributed to derivation from continental sources via glacial erosion (Biscaye, 1965; Griffin et al., 1968). Kaolinite is highly concentrated in the tropical Atlantic, and its presence is attributed to extreme chemical weathering in tropical environments. A first-order observation of the kaolinite/chlorite ratio in Atlantic sediments is therefore that there is a strong trend with latitude of the distribution (Fig. 1) that can be simply related to the chemical weathering intensity (Biscaye, 1965). Chemical weathering is more prominent in the tropics while physical weathering dominates at higher latitudes. It is also noticeable in Fig. 1 that the isopleths of kaolinite/chlorite do not strictly follow latitudinal bands. Rather they are systematically displaced in accord with the main wind and surface ocean currents, and are also dispersed by bottom currents where they are strong (Innocent et al., 2000). The extensive survey of the South Atlantic and the Atlantic sector of the Southern Ocean (Petschick et al., 1996) further emphasizes the geographical similarity

of clay provinces and wind and ocean circulation patterns. Although Petschick et al. (1996) interpreted their results almost exclusively as the result of bottom current movements, the patterns have a strong resemblance to winds and surface ocean currents of the region (Franzese and Hemming, 2013).

2.2. Pathways of sediment supply to the Atlantic Ocean

In general, terrigenous sediments are formed by weathering of exposed rocks on the continents, although the areas of the catchments are not quantitatively represented in terms of their fractional contributions (Cook et al., 2017; Garzanti et al., 2009; Licht and Hemming, 2017; Moecher and Samson, 2006). Sediments derived from the continents are delivered to the ocean by wind, water, and ice, and are redistributed within the ocean by surface and bottom currents. Where there are glaciers in the source catchment, especially temperate glaciers, they are large contributors to sediment supply. Rivers are the dominant source of sediment to the ocean margins in most parts of the world except near major deserts and ice sheets, and the supply of sediments from rivers depends on the characteristics of the river catchment such as precipitation/runoff, area, and topography (Milliman and Meade, 1983; Milliman and Syvitski, 1992). Although it is difficult to get an accurate estimate of natural suspended sediment flux to the ocean due to lack of data as well as interference from land usage and dams, Milliman and Meade (Milliman and Meade, 1983) provided a synthesis of riverine sediment supply to the ocean. The Amazon River is, by far, the largest sediment supplier to the Atlantic Ocean. The sediment discharge from the northern rivers in South America (which includes the Amazon and Orinoco) is 1438 million tons per year. Mexico and Central America collectively discharge 442 million tons per year, and southern South American rivers discharge 154 million tons per year. In contrast North America, Europe and Africa have much smaller discharges, with 30 million tons per year from Northeast Canada, 17 million tons per year from the U.S. Atlantic coast, 31 million tons per year from Western Europe, and 240 million tons per year from all along the western side of Africa. The sediment yield of a river, the discharge divided by the drainage area, in general is smaller for larger rivers (Milliman and Meade, 1983), so the assessment of only the largest rivers, while necessary due to data availability, may underestimate the sediment being supplied to the ocean, and importantly may miss the texture of provenance changes from different drainage catchments. For example, the digitate pattern of illite concentrations near the eastern coast of South America appears to reflect local input from a series of rivers (Griffin et al., 1968).

In polar regions glaciers can be important contributors to marine sediments, either due to direct deposition where glaciers advance beyond the coastline, or due to icebergs that calve off and melt and thus drop ice rafted detritus on the ocean floor (e.g., Ruddiman, 1977). In very dry regions, wind-blown sediment can make up a substantial portion of marine sediments (Griffin et al., 1968).

Griffin et al. (1968) identified several places in the world's ocean where the composition of clays is inconsistent with known local river sediment compositions, and clays in these areas are likely deposited by winds. The middle of the North Pacific gyre is a particularly good example of sediment supply that is clearly transported by winds (Griffin et al., 1968; Jones et al., 1994; Nakai et al., 1993; Pettke et al., 2000; Rea et al., 1985). In the Atlantic basin, two of these are the area of high kaolinite concentration in the subtropical Atlantic (considered to be likely derived from the Sahara), and the area of high illite concentration in the eastern North Atlantic (considered by Griffin et al. (Griffin et al., 1968) to be likely delivered by winds sourced from North America). Grousset et al. (Grousset et al., 1988) also concluded a substantial wind-blown dust source from North America based on the occurrence of relatively low ε_{Nd} in eastern North Atlantic core tops at ~45°N. While these sediments likely originated from old continental sources from the Canadian Shield or Greenland, it seems probable that they were transported by icebergs based on the mapping of ice rafted detritus in the North Atlantic (Ruddiman, 1977).

2.3. Factors controlling sediment composition

Weathering acts to break rocks down into small particles through a combination of physical and chemical processes, and the composition of the resulting sedimentary material will vary depending on the composition of the source, as well as the style and intensity of weathering. The chemical index of alteration (Nesbitt and Young, 1984) is a powerful geochemical measure of weathering intensity. CIA is $100 * Al_2O_3 / (Al_2O_3 + Na_2O + CaO + Na_2O)$, in molar proportions and not including carbonate or sea salt. Catchments with high sediment yield due to high denudation rates will have low CIA (McLennan, 1993) and their compositions will be close to those of their sources. On the other extreme, sediments derived from low relief regions in humid tropical environments will have high CIA and lower sediment yield. The parent and daughter elements of radiogenic isotope systems will also vary according to these rules, which minerals are their main hosts, and the stability during weathering of those minerals.

All sediment provenance approaches depend on characterizing any systematic variation of the compositions of potential sources, such as rock type or age, as well as the behavior of the mineralogical or geochemical system employed. Much of the continental crust has a veneer of sedimentary strata (Fig. 2a), and those sedimentary materials are likely to be large contributors to the next generation of sediments (e.g., review in (Taylor and McLennan, 1985)). This recycling of sedimentary materials leads to some extra layers of reasoning required to apply weathering and source tracers to sediment records (e.g., Thiry, 2000).

Geologic maps provide important hints about the provenance characteristics of sediments that might be derived from them, but it must be remembered that different aspects of the geological history are expressed differently depending on the rock types exposed on the landscape. Standard maps usually attempt to document rock types and their formation ages. In other words, they tend to document crystallization ages for igneous rocks, depositional ages for sedimentary rocks, and (less consistently) metamorphic ages for metamorphic rocks. This is very helpful, but it does not capture the pre-history of the igneous and sedimentary rocks (what rock types and which range of ages for their sources?), which is important for radiogenic isotope systems, nor does it capture the thermochronological history after the rocks formed. For example, where they are found, zircons provide the most reliable measure of crystallization age of igneous rocks or timing of high grade metamorphic zircon growth with the U−Pb chronometer (Gehrels, 2014; Mezger and Krogstad, 1997), so if such ages are available that is what would be estimated on geologic maps of igneous and high grade metamorphic rocks. However, these same zircons would likely give younger ages for fission track and (U−Th)/He in most rocks due to the lower retention of tracks and helium in zircon (Reiners et al., 2005a; Tochilin et al., 2012). K-bearing minerals tend to have intermediate closure temperatures between 200° and 500 °C (Reiners et al., 2005b), and thus in many cases would yield ages that are significantly younger than U−Pb zircon from the same rock. And it is a real complication that continents are mostly covered in a sedimentary veneer. Zircons are extremely resistant to breaking down, so they tend to survive multiple weathering, transport and deposition in the sedimentary system (Hurbert, 1962). In contrast, K-bearing minerals tend to break down during weathering (Goldich, 1938) and diagenesis (Aronson and Hower, 1976) so they are not likely to be found in recycled sediment sources, except for muscovite and illite (Clauer and Chaudhuri, 1995; Hurley et al., 1961).

Simplified geologic maps of the sedimentary cover (Fig. 2a), crystalline basement (Fig. 2b) and volcanic rocks (Fig. 2c) for the continents surrounding the Atlantic Ocean reveal that all of the continents contain a large range of geologic ages of crystalline basement as well as sedimentary cover. The data presented here are placed on a compiled

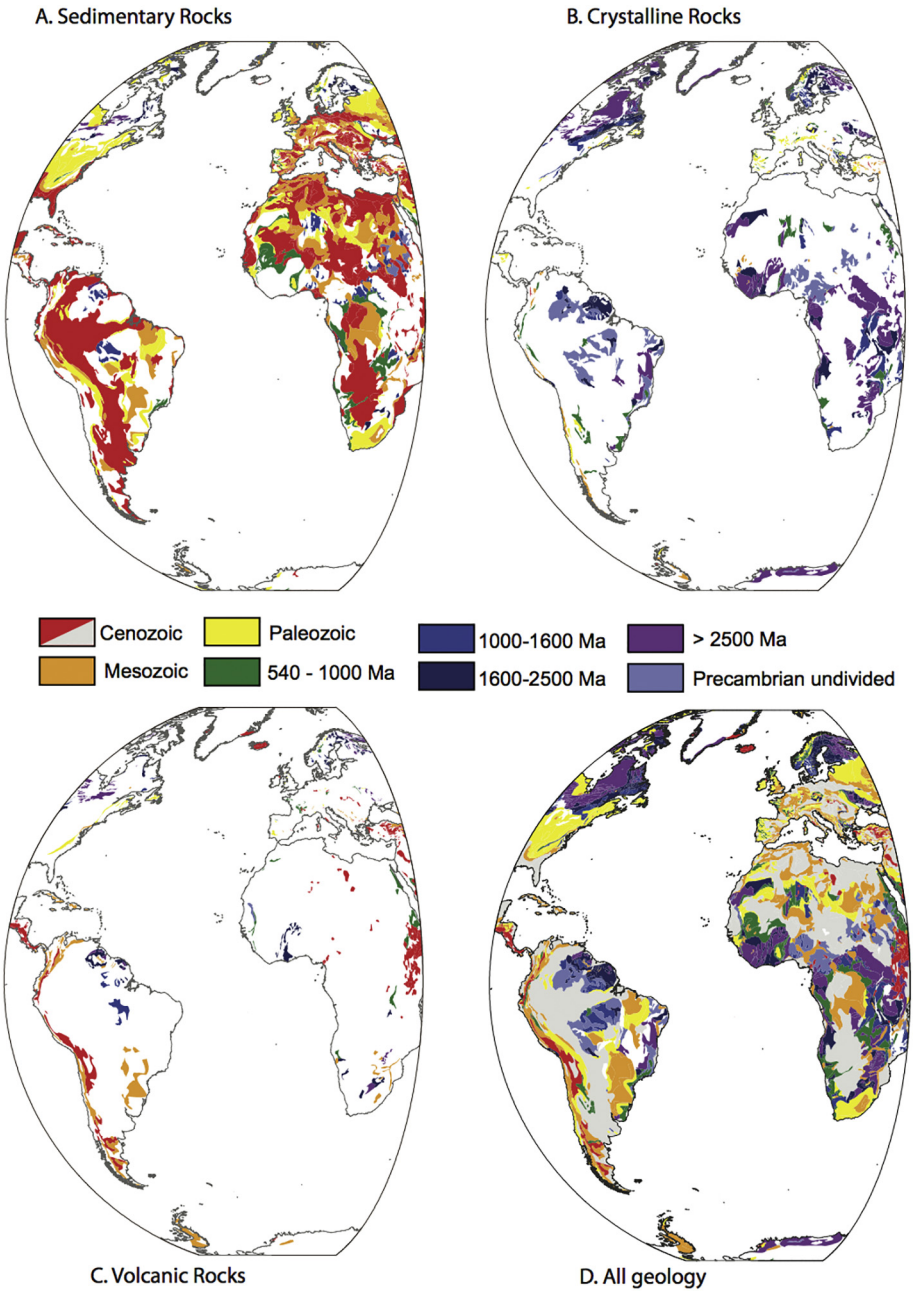

Fig. 2. Geologic maps of the continents surrounding the Atlantic Ocean taken from Generalized geological map of the world, Geological Survey of Canada Open File 2915D. Ages are colour coded according to the rainbow, where red is young and violet is old in order to match with the radiogenic isotope data plotted in Fig. 6. A) Distribution of sedimentary rocks of different geologic ages; B) Distribution of crystalline rocks of different geologic ages; C) Distribution of volcanic rocks of different geologic ages; D) Generalized geology – Cenozoic sedimentary rocks are shown as gray in this figure, whereas in the sedimentary rock map they are shown as red – this is because for the comparison with radiogenic isotopes young sedimentary rocks will simply be reflecting the isotopic character of their sources.

geologic map (Figs. 2d, 3a, b, c) in which the sedimentary rocks are shown as gray regardless of their depositional age because sedimentary rocks will largely reflect the geologic history of the crystalline and volcanic rocks from which they are derived. As a primary observation, there is much more extensive exposure of very old crystalline basement in the North Atlantic region compared to the rest of the continental area surrounding the basin. And there is much more extensive exposure of very young source terrains in southern South America and the Antarctic Peninsula. This range of geologic ages is expected to be broadly reflected in the radiogenic isotope systems of Atlantic Ocean terrigenous sediments.

2.4. Samples and methods

The new $^{40}Ar^{*}$ data presented here are from two sets of samples. The primary batch is a subset of the near-surface samples taken by Biscaye (1965) for his Ph.D. thesis completed at Yale in 1964. Biscaye sampled cores as they were coming in from Lamont cruises during the 1960's, and in many cases, he was able to obtain the core-tops for his survey. Biscaye carefully archived his collections of < 2 μm and 2–20 μm fractions on glass XRD slides, providing a phenomenal resource for future studies. I have made an initial survey of the < 2 μm fractions of samples from the Biscaye clay mineral study (Fig. 1, Table 1). The samples were gently scraped onto weighing paper from the XRD mounts using a razor blade, placed in 1.5 ml microcentrifuge tubes, dispersed in dionized water, and centrifuged. Excess water was pipetted off and the samples were dried in an oven at 60 °C to form clods at the bottoms of the microcentrifuge tubes. Clods were weighed with a microbalance, and ranged from 0.5 to 5.4 mg (Table 2).

The other set is Holocene and Last Glacial Maximum (LGM) samples from along the axis of the mid-Atlantic Ridge (MAR). The MAR samples (Table 3) were selected from the Lamont core repository, and carbonate concentrations and radiocarbon of the bulk samples were used for the stratigraphic control (Wally Broecker, personal communication). Samples were dispersed and wet-sieved at 63 μm. The fine fractions were leached to remove calcium carbonate and ferromanganese fractions

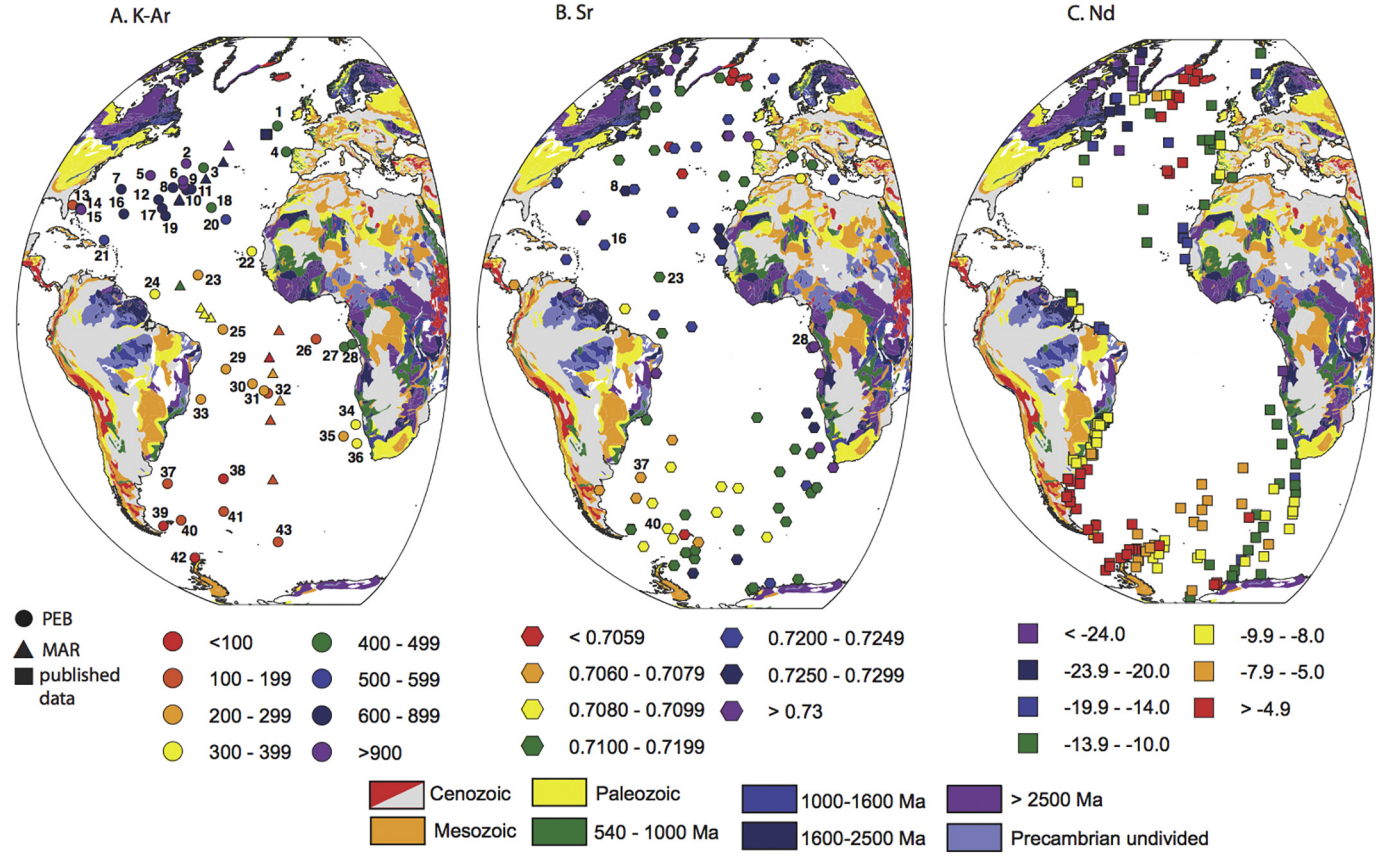

Fig. 3. Generalized geology map of the land surrounding the Atlantic Ocean with radiogenic isotope data from terrigenous marine sediments. 6a Map of K/Ar ages in the Atlantic Ocean. Data sources: this study (circles, numbered as in Table 2), published studies (triangles) (S R Hemming et al., 2002; Huon and Ruch, 1992; Hurley et al., 1963a; Jantschik and Huon, 1992). Fig. 6b Map of $^{87}Sr/^{86}Sr$ of terrigenous sediments in the Atlantic Ocean. Numbers refer to samples with $^{40}Ar^*$ data in Table 2. Data sources: (Aarons et al., 2013; Cole et al., 2009; Dasch, 1969; DePaolo et al., 2006; Farmer et al., 2003; Franzese et al., 2009; Huon and Jantschik, 1993; Kumar et al., 2014; McLennan et al., 1990; Meyer et al., 2011; Noble et al., 2012; Revel et al., 1996; Reyes et al., 2014; Rutberg et al., 2000; Skonieczny et al., 2013; Walter et al., 2000). Fig. 6c Map of ε_{Nd} of terrigenous sediments in the Atlantic Ocean. Data sources (Aarons et al., 2013; Basile et al., 1997; Cole et al., 2009; de Mahiques et al., 2008; Fagel and Mattielli, 2011; Grousset and Biscaye, 1989; Hegner et al., 2007; Innocent et al., 1997, 2000; Kumar et al., 2014; McLennan et al., 1990; Meyer et al., 2011; Noble et al., 2012; Reyes et al., 2014; Skonieczny et al., 2013; Toucanne et al., 2015; Walter et al., 2000; Zhang et al., 2015).

using the procedure of Rutberg et al. (2000), modified from Biscaye (1965) by replacing his sodium dithionate reagent for ferromanganese leaching with a hydroxylamine hydrochloride reagent as developed by Chester and Hughes (1969). Following this leaching the bulk < 63 μm terrigenous sediment was dispersed in deionized water and clods prepared and weighed as described for the Biscaye samples.

Weighed clods were loaded into pits in 21-spot disks that included three GLO-1 standards (Odin, 1976) and 18 unknowns. Argon concentrations and $^{40}Ar/^{36}Ar$ ratios were measured on the samples and GLO-1, interspersed with measurements of backgrounds and diluted atmospheric argon from an air pipette that dispensed a constant amount of approximately 4×10^{-14} mol of argon. Measurements were made on a VG5400 noble gas mass spectrometer in the AGES (Argon Geochronology for Earth Sciences) laboratory at Lamont-Doherty Earth Observatory with multiplier in analogue mode. The air pipette, solid standards and unknown measurements were corrected for backgrounds estimated from the most recent preceding blank measurement. The data were normalized to the air pipette measurements made during each batch (where a batch is all of the analyses made between venting and pumping two consecutive disks). Weighed samples of GLO-1 glauconite standard (Derkowski et al., 2009; Odin, 1976) and SCO-1 sediment were used to calibrate for concentration of the air pipette standard and test for replicability of similar samples respectively (Hemming et al., 2002). The samples reported here were run shortly after the North Atlantic samples reported in Hemming et al. (2002), and the precisions are not as good as found in the North Atlantic project. Since that time, we have improved the measurement strategy, and we correct for instrument drift using the time series of measured airs (Gombiner et al., 2016), which has improved the measurement uncertainty to about 1–2% for air and GLO-1 measurements, but during the time of the analyses reported here, corrections were made only to the average measured air for each batch. During the interval of these analyses (2002 − 2003), the signal on the air pipette was 0.661 nannoamps ± 6.5% and the $^{40}Ar/^{36}Ar$ of the air pipette was 290.12 ± 0.9%. Duplicate aliquots of each sample reported here were within 20% of each other for all the Biscaye samples except one, which is the youngest of the Biscaye samples, and has duplicate measurements that are 12 m.y. apart (28%). Measurements are reported in Tables 2 and 3. The average of the two reported analyses is used with the estimated % error being 100× difference between the two runs ÷ the average of the two runs. This is, in effect, a 2-sigma error estimate, and the average error calculated in this way is consistent with that estimated from the reproducibility of the air pipettes. Duplicate aliquots of most of the MAR samples are within 20% of each other, but some had considerably larger differences (up to 40%). Except for one sample, RC24-10 Holocene, more replicates were analyzed for samples that had differences greater that 20%, and some samples were analyzed four times.

Ages were calculated using the decay constants of Steiger and Jager (1977). Although the major element compositions would further yield direct comparisons of weathering proxies from elemental and mineralogical approaches in addition to K concentrations for calculating the K/Ar ages, for the purposes of this paper a 2 wt% K concentration is

Table 1
Locations of samples analyzed with clay mineral data from Biscaye (1965).

Core	Map number	Latitude	Longitude	Water depth (m)	%Montmorillonite	%Illite	%Kaolinite	%Chlorite
R5-37, ~10 cm	1	49.90	−15.55	4565	24	54	10	12
A180-9, 0 cm	2	39.45	−45.95	4060	10	68	6	16
A180-16, 0 cm	3	38.35	−39.48	2270	26	54	10	10
R5-45, 0 cm	4	42.69	−11.08	1865	11	72	11	6
VM16-211, 5 cm	5	36.30	−57.00	5267	9	63	10	18
VM17-166, 0 cm	6	34.93	−45.35	4211	6	69	10	15
A164-36, 0 cm	7	32.72	−65.27	4515	11	65	10	14
A153-144, 0 cm	8	33.13	−48.13	4850	16	62	10	12
A153-146,10 cm	9	33.71	−44.74	4050	8	66	10	16
A153-148, 0 cm	10	32.57	−43.48	3300	10	66	12	12
VM17-165, 0 cm	11	32.75	−41.90	3925	10	65	12	13
VM16-209, 0 cm	12	30.00	−51.87	4673	10	64	12	14
VM12-129, ~20 cm	13	28.63	−79.40	811	62	24	10	4
VM15-201, 0 cm	14	27.87	−76.55	4759	13	57	14	16
VM15-199, 9 cm	15	27.48	−76.08	4857	11	62	12	15
A181-10, 10 cm	16	26.40	−61.93	5855	11	63	16	10
VM16-208, 0 cm	17	27.73	−49.92	4861	7	68	11	14
VM17-163, 0 cm	18	27.97	−34.13	5132	6	64	22	8
VM16-207, 0 cm	19	25.85	−48.38	4825	11	69	12	8
VM17-162, 0 cm	20	24.97	−28.93	5485	12	58	25	5
A172-9, 0 cm	21	19.80	−66.18	7955	18	55	14	13
VM17-159, 0 cm	22	16.98	−20.05	46	26	43	27	4
VM12-7, 10 cm	23	11.20	−36.02	5444	33	32	30	5
A181-5, 2 cm	24	6.53	−48.72	3865	25	51	18	6
A180-79, 0 cm	25	−2.07	−28.18	5100	36	42	20	2
VM12-78	26	−4.38	−0.18	4232	34	39	35	3
VM12-75, ~10 cm	27	−6.31	8.32	4022	32	27	39	2
VM12-72, ~10 cm	28	−5.63	10.66	2107	30	29	39	2
VM16-30	29	−11.73	−27.62	5513	14	60	20	6
VM16-33	30	−15.33	−19.72	4357	40	40	12	8
VM16-34	31	−17.03	−16.22	3530	20	48	22	10
VM16-35	32	−17.67	−15.10	3892	24	49	18	9
A180-105, 0 cm	33	−19.17	−35.98	3840	16	31	50	3
VM12-62	34	−25.50	12.45	3036	13	76	5	6
VM12-61, 10 cm	35	−28.47	8.70	5064	28	60	6	6
VM12-60	36	−30.33	13.17	3111	21	69	6	4
VM12-53	37	−40.90	−53.26	3797	24	57	6	13
VM12-52	38	−39.60	−32.88	5009	42	40	5	13
VM14-42	39	−52.75	−62.97	316	22	51	3	24
VM17-107	40	−51.13	−54.37	1525	18	54	3	25
VM17-124	41	−48.57	−36.07	5172	27	49	4	20
VM17-96	42	−62.55	−59.43	584	57	15	2	26
VM14-57	43	−57.57	−17.10	4978	33	37	3	27

assumed for all the samples.

3. Results

The K/Ar age data from the Biscaye samples are reported in Table 2 and shown in map view in Fig. 3a. Those from the MAR samples are reported in Table 3, and the Holocene data are shown in map view in Fig. 3a. The range of $^{40}Ar^*$ concentrations is 1.3×10^{-13} to 6.5×10^{-12} mol/mg. With the assumed 2 wt% K, this yields a range of estimated K/Ar ages of 44 ± 12 Ma for the sample with youngest provenance in the southwest Atlantic to 1231 ± 116 Ma for the sample with oldest provenance in the northwest Atlantic. There is an increase in age from south to north along the western Atlantic, with the exception of sample VM12–129 off Florida, which has an anomalously young age of 169 ± 8 Ma. This sample comes from ~20 cm depth in the core, so not exactly surface sediment. In the South Atlantic four samples within the Argentine Basin yield similar ages between ~140 and 150 Ma, while one on the northeastern flank of the basin yields the youngest age of the sample set. A sample from near the Antarctic Peninsula yields 63 ± 9 Ma, and a sample from the Argentine shelf at 52.75°S yields 93 ± 13 Ma. Between 30°S and the equator, ages in the eastern basin (200–300 Ma) are older than those in the western basin (50–200 Ma). North of 20°N, with the exception of the anomaly noted above, K/Ar ages west of the mid-Atlantic ridge are significantly older (> 700 Ma) than those east of the ridge (300–500 Ma).

4. Discussion

4.1. The K/Ar distribution of terrigenous sediments in the Atlantic Ocean

In contrast to the strong climate-zone-correlated distribution of kaolinite/chlorite in Atlantic sediments (Fig. 1), the radiogenic isotope compositions are more influenced by the geology of the surrounding continents (Figs. 3, 4). Data for kaolinite/chlorite (***a***), K/Ar (***b***), $^{87}Sr/^{86}Sr$ (***c***) and ε_{Nd} (***d***) are presented against latitude in Fig. 4, separated into eastern and western basins relative to the MAR. Overall the western basin samples show a strong and simple increase in K/Ar age with increasing northward latitude, with the youngest samples from near the southern tip of South America between 60°S and 40°S.

The K/Ar age values have a pattern that resembles that found for the Nd isotopes (Figs. 3, 4) with oldest K/Ar and lowest ε_{Nd} in the northwest Atlantic and youngest K/Ar and highest ε_{Nd} in the southwest Atlantic. Intermediate values are found in the tropical belt as well as off the coast of Europe (Figs. 3, 4). This general trend in sediment compositions matches the known geology of the continental sources around the Atlantic basin (Figs. 2, 3) with extreme old ages in Canada and Greenland and extreme young ages in active tectonic settings like the southern tip of South America, Antarctic Peninsula and the Scotia Arc.

Table 2
Argon data from Biscaye (1965) samples.

	Core	Map number	Sample weight (mg)	40Ar (namps)	40Ar* (namps)	% 40Ar*	40Ar* (namps/mg)	40Ar* (mol/mg)	40K/mg (2%K)	K/Ar Age (Ma)	Average	%diff	± (Ma)
1	A153-144, 0 cm	8	3.331	111.9	104.5	93	31	3.78E-12	5.97E-11	832.7	787	12	92
2	A153-144, 0 cm		2.020	59.1	54.9	93	27	3.27E-12	5.97E-11	740.3			
3	A153-146,10 cm	9	3.166	124.2	117.1	94	37	4.46E-12	5.97E-11	949.1	935	3	28
4	A153-146,10 cm		2.183	82.8	77.7	94	36	4.29E-12	5.97E-11	920.7			
5	A153-148, 0 cm	10	2.453	69.1	63.3	92	26	3.11E-12	5.97E-11	710.3	723	3	24
6	A153-148, 0 cm		2.360	69.2	63.5	92	27	3.24E-12	5.97E-11	734.7			
7	A164-36, 0 cm	7	2.646	93.0	86.3	93	33	3.93E-12	5.97E-11	859.1	845	3	28
8	A164-36, 0 cm		1.605	54.7	50.3	92	31	3.77E-12	5.97E-11	831.0			
9	A172-9, 0 cm	21	2.461	51.8	46.2	89	19	2.26E-12	5.97E-11	542.0	554	4	25
10	A172-9, 0 cm		2.903	64.0	57.2	89	20	2.38E-12	5.97E-11	566.8			
11	A180-105, 0 cm	33	3.008	29.7	24.5	83	8	9.81E-13	5.97E-11	255.3	254	1	2
12	A180-105, 0 cm		3.912	37.7	31.6	84	8	9.74E-13	5.97E-11	253.6			
13	A180-16, 0 cm	3	2.631	43.4	35.6	82	14	1.63E-12	5.97E-11	406.5	393	7	27
14	A180-16, 0 cm		2.727	41.8	34.2	82	13	1.51E-12	5.97E-11	379.4			
20	A180-79, 0 cm	25	2.520	24.9	20.3	82	8	9.7E-13	5.97E-11	252.6	259	5	12
21	A180-79, 0 cm		3.975	41.1	33.6	82	8	1.02E-12	5.97E-11	264.8			
22	A180-9, 0 cm	2	2.081	107.1	98.9	92	48	5.73E-12	5.97E-11	1148.4	1206	10	115
23	A180-9, 0 cm		2.439	143.0	132.1	92	54	6.53E-12	5.97E-11	1263.5			
24	A181-10, 10 cm	16	3.452	99.0	91.9	93	27	3.21E-12	5.97E-11	729.1	705	7	47
25	A181-10, 10 cm		3.470	92.2	85.2	92	25	2.96E-12	5.97E-11	681.7			
26	A181-5, 2 cm	24	4.533	59.9	51.5	86	11	1.37E-12	5.97E-11	347.4	353	3	12
27	A181-5, 2 cm		4.247	57.4	49.9	87	12	1.42E-12	5.97E-11	358.9			
28	R5-37, ~10 cm	1	2.101	38.8	34.7	89	17	1.99E-12	5.97E-11	485.2	458	12	54
29	R5-37, ~10 cm		1.606	26.9	23.2	87	14	1.74E-12	5.97E-11	430.9			
30	R5-45, 0 cm	4	1.581	21.9	19.3	88	12	1.47E-12	5.97E-11	370.3	398	14	56
31	R5-45, 0 cm		2.292	36.4	32.6	90	14	1.72E-12	5.97E-11	426.5			
36	VM12-129, ~20 cm	13	1.775	12.8	9.3	73	5	6.32E-13	5.97E-11	168.5	165	5	8
37	VM12-129, ~20 cm		2.123	14.6	10.6	73	5	6.01E-13	5.97E-11	160.6			
40	*VM12-52*	*38*	*1.421*	*5.4*	*1.6*	*29*	*1*	*1.33E-13*	*5.97E-11*	*36.8*	43	28	12
41	*VM12-52*		*1.309*	*3.3*	*1.9*	*59*	*1*	*1.76E-13*	*5.97E-11*	*48.5*			
42	VM12-53	37	0.890	7.5	3.7	50	4	5.08E-13	5.97E-11	136.7	136	2	2
43	VM12-53		0.989	8.1	4.1	51	4	4.99E-13	5.97E-11	134.3			
45	VM12-60	36	0.825	9.8	7.3	75	9	1.07E-12	5.97E-11	276.8	292	11	31
46	VM12-60		3.441	44.2	34.2	77	10	1.2E-12	5.97E-11	307.7			
47	VM12-61, 10 cm	35	2.797	35.2	25.7	73	9	1.11E-12	5.97E-11	286.4	267	15	39
48	VM12-61, 10 cm		3.844	42.9	30.3	71	8	9.49E-13	5.97E-11	247.5			
49	VM12-62	34	0.941	17.5	10.0	57	11	1.28E-12	5.97E-11	326.5	331	3	9
50	VM12-62		2.465	45.9	26.9	59	11	1.32E-12	5.97E-11	335.8			
51	VM12-7, 10 cm	23	1.890	18.1	13.6	75	7	8.68E-13	5.97E-11	227.7	212	15	32
52	VM12-7, 10 cm		1.065	9.0	6.5	73	6	7.40E-13	5.97E-11	195.8			
53	VM12-72, ~10 cm	28	1.833	34.0	29.7	87	16.196	1.95E-12	5.97E-11	476.6	459	8	35
54	VM12-72, ~10 cm		2.757	46.8	40.9	87	14.826	1.79E-12	5.97E-11	441.9			
55	VM12-75, ~10 cm	27	2.502	38.3	34.8	91	13.918	1.68E-12	5.97E-11	417.6	416	1	2
56	VM12-75, ~10 cm		2.288	34.9	31.5	91	13.833	1.67E-12	5.97E-11	415.4			
57	VM12-78	26	1.061	7.9	5.8	73	5.452	6.57E-13	5.97E-11	174.9	183	8	15
58	VM12-78		0.713	9.0	4.2	47	5.96	7.18E-13	5.97E-11	190.3			
63	VM14-42	39	0.575	2.5	1.5	59	2.544	3.07E-13	5.97E-11	83.8	90	14	12
64	VM14-42		1.828	8.8	5.4	61	2.927	3.53E-13	5.97E-11	96.1			
69	VM14-57	43	1.153	13.3	5.0	38	4.38	5.28E-13	5.97E-11	141.9	145	5	7
70	VM14-57		1.876	20.5	8.6	42	4.596	5.54E-13	5.97E-11	148.6			
77	VM15-199, 9 cm	15	1.884	67.4	63.1	94	33.488	4.04E-12	5.97E-11	878.1	898	4	39
78	VM15-199, 9 cm		3.286	123.8	116.4	94	35.436	4.27E-12	5.97E-11	917.4			
79	VM15-201, 0 cm	14	1.889	71.4	65	91	34.431	4.15E-12	5.97E-11	897.0	877	5	40
80	VM15-201, 0 cm		2.272	81.0	73.9	91	32.504	3.92E-12	5.97E-11	857.3			

(*continued on next page*)

Table 2 (*continued*)

	Core	Map number	Sample weight (mg)	40Ar (namps)	40Ar* (namps)	% 40Ar*	40Ar* (namps/mg)	40Ar* (mol/mg)	40K/mg (2%K)	K/Ar Age (Ma)	Average	%diff	± (Ma)
81	VM16-207, 0 cm	19	2.532	75.2	70.2	93	27.744	3.34E-12	5.97E-11	753.3	756	1	6
82	VM16-207, 0 cm		4.017	120.4	112.4	93	27.991	3.37E-12	5.97E-11	758.8			
83	VM16-208, 0 cm	17	1.822	49.6	45.9	93	25.203	3.04E-12	5.97E-11	697.0	729	9	64
84	VM16-208, 0 cm		3.192	96.5	89.7	93	28.083	3.38E-12	5.97E-11	760.6			
85	VM16-209, 0 cm	12	2.072	68.2	63.5	93	30.669	3.70E-12	5.97E-11	818.6	808	3	22
86	VM16-209, 0 cm		1.285	41.1	38.2	93	29.69	3.58E-12	5.97E-11	797.1			
87	VM16-211, 5 cm	5	1.921	91.5	86.4	94	44.949	5.42E-12	5.97E-11	1101.7	1075	5	53
88	VM16-211, 5 cm		0.000	80.7	76.1	94	42.16	5.08E-12	5.97E-11	1049.1			
89	VM16-30	29	1.003	9.1	7.4	82	7.401	8.92E-13	5.97E-11	233.6	245	9	22
90	VM16-30		3.062	29.3	25	85	8.148	9.82E-13	5.97E-11	255.6			
95	VM16-33	30	1.457	12.3	9.5	77	6.499	7.83E-13	5.97E-11	206.6	226	18	40
96	VM16-33		0.705	7.3	5.5	76	7.832	9.44E-13	5.97E-11	246.3			
97	VM16-34	31	0.930	8.3	6.5	79	7.009	8.45E-13	5.97E-11	222.0	207	14	29
98	VM16-34		0.969	8.0	5.8	73	6.032	7.27E-13	5.97E-11	192.6			
99	VM16-35	32	0.654	5.2	3.7	71	5.668	6.83E-13	5.97E-11	181.5	186	4	8
100	VM16-35		0.816	6.5	4.8	75	5.93	7.15E-13	5.97E-11	189.6			
112	VM17-107	40	2.387	42.7	10.4	24	4.407	5.31E-13	5.97E-11	142.6	143	1	1
113	VM17-107		2.374	41.3	10.5	26	4.44	5.35E-13	5.97E-11	143.7			
114	VM17-124	41	1.829	26.3	8.6	33	4.725	5.70E-13	5.97E-11	152.7	140	18	25
115	VM17-124		3.075	34.2	12	35	3.916	4.72E-13	5.97E-11	127.3			
118	VM17-159, 0 cm	22	2.082	25.1	20.7	82	9.94	1.20E-12	5.97E-11	307.7	325	11	35
119	VM17-159, 0 cm		2.013	26.8	22.6	84	11.206	1.35E-12	5.97E-11	342.8			
120	VM17-162, 0 cm	20	1.974	37.8	33.1	88	16.75	2.02E-12	5.97E-11	491.6	503	5	23
121	VM17-162, 0 cm		2.779	55.8	49.2	88	17.695	2.13E-12	5.97E-11	514.9			
122	VM17-163, 0 cm	18	2.896	50.4	45.3	90	15.628	1.88E-12	5.97E-11	461.5	466	2	9
123	VM17-163, 0 cm		1.982	35.6	31.6	89	15.943	1.92E-12	5.97E-11	470.1			
124	VM17-165, 0 cm	11	1.972	60	53.7	89	27.214	3.28E-12	5.97E-11	742.2	731	3	22
125	VM17-165, 0 cm		1.608	47.1	42.1	89	26.187	3.16E-12	5.97E-11	719.7			
126	VM17-166, 0 cm	6	2.633	113.3	105.8	93	40.19	4.84E-12	5.97E-11	1011.1	1005	1	13
127	VM17-166, 0 cm		1.928	81.5	76.1	93	39.456	4.76E-12	5.97E-11	998.2			
131	VM17-96	42	0.808	4.4	1.4	31	1.706	2.06E-13	5.97E-11	56.7	61	15	9
132	VM17-96		1.844	10.4	3.6	35	1.979	2.39E-13	5.97E-11	65.6			

Table 3
Argon data from mid-Atlantic ridge samples.

Core	Time period	Latitude (deg. N)	Longitude (deg. E)	Sample weight (mg)	40Ar (namps)	40Ar* (namps)	% 40Ar*	40Ar* (namps/mg)	40Ar* (mol/mg)	40Ar* average	%diff	K/Ar age (Ma)	± (Ma)
VM28-89	Holocene	44.5	−32.60	0.938	38	36	95	38	4.63E-12	4.67E-12	1.7	998.4	11.9
VM28-89	Holocene	44.5	−32.60	1.290	53	50	95	39	4.71E-12				
VM30-96	Holocene	40	−33.10	1.098	28	24	86	22	2.66E-12	2.72E-12	4.4	639.4	19.9
VM30-96	Holocene	40	−33.10	0.913	23	21	91	23	2.78E-12				
VM30-94TW	Holocene	35.5	−37.80	1.826	51	41	81	22	2.71E-12	2.99E-12	18.6	648.9	85.1
VM30-94TW	Holocene	35.5	−37.80	2.109	68	57	84	27	3.26E-12				
VM26-16(p)	Holocene	30.2	−45.10	1.083	29	25	85	23	2.75E-12	2.74E-12	3.0	657.1	21.1
VM26-16(p)	Holocene	30.2	−45.10	0.721	21	16	74	22	2.67E-12				
VM26-16(p)	Holocene	30.2	−45.10	3.070	94	68	73	22	2.67E-12				
VM26-16(p)	Holocene	30.2	−45.10	2.911	92	69	75	24	2.86E-12				
VM26-17	Holocene	29.9	−45.10	1.352	27	24	91	18	2.18E-12	2.22E-12	3.5	538.6	13.4
VM26-17	Holocene	29.9	−45.10	1.350	27	25	94	19	2.26E-12				
VM22-26A(p)	Holocene	8.7	−41.30	3.809	89	54	61	14	1.70E-12	1.75E-12	5.3	433.3	16.2
VM22-26A(p)	Holocene	8.7	−41.30	3.877	86	58	67	15	1.79E-12				
VM25-60	Holocene	3.3	−34.80	1.315	23	15	66	12	1.41E-12	1.33E-12	11.3	366.1	29.2
VM25-60	Holocene	3.3	−34.80	1.280	19	13	70	10	1.26E-12				
RC13-88	Holocene	1.8	−33.70	1.328	27	16	60	12	1.46E-12	1.40E-12	9.6	379.3	25.7
RC13-88	Holocene	1.8	−33.70	1.320	24	15	61	11	1.33E-12				
VM22-32	Holocene	0.9	−31.80	1.461	29	16	57	11	1.33E-12	1.27E-12	10.4	348.6	25.6
VM22-32	Holocene	0.9	−31.80	0.822	20	8	40	10	1.20E-12				
RC24-10	Holocene	−2.2	−11.30	1.391	17	6	35	4	5.09E-13	4.33E-13	34.8	140.9	34.7
RC24-10	Holocene	−2.2	−11.30	0.817	9	2	28	3	3.58E-13				
VM22-175	Holocene	−8.8	−14.30	0.926	15	3	19	3	3.56E-13	4.23E-13	39.7	99.8	21.1
VM22-175	Holocene	−8.8	−14.30	1.097	22	5	22	4	5.24E-13				
VM22-175(p)	Holocene	−8.8	−14.30	1.185	16	4	23	3	3.88E-13				
RC16-77(p)	Holocene	−12.7	−13.40	1.399	64	12	18	8	1.00E-12	1.21E-12	9.6	267.6	59.1
RC16-77(p)	Holocene	−12.7	−13.40	1.015	47	9	20	9	1.12E-12				
RC16-77(p)	Holocene	−12.7	−13.40	0.954	37	12	33	13	1.51E-12				
VM16-36A	Holocene	−19.4	−11.40	0.960	8	7	84	7	8.41E-13	7.71E-13	18.1	227.3	29.1
VM16-36A	Holocene	−19.4	−11.40	0.956	7	6	82	6	7.01E-13				
RC8-19	Holocene	−24.3	−14.70	1.116	6	5	77	4	5.28E-13	5.44E-13	6.0	146.0	6.2
RC8-19	Holocene	−24.3	−14.70	1.157	7	5	75	5	5.60E-13				
RC12-292(p)	Holocene	−39.7	−15.50	2.043	21	6	29	3	3.62E-13	3.76E-13	7.5	101.5	5.4
RC12-292(p)	Holocene	−39.7	−15.50	2.255	23	7	31	3	3.91E-13				
VM30-96A	Glacial	40	−33.10	1.048	21	20	94	19	2.25E-12	2.63E-12	22.3	555.0	68.2
VM30-96A	Glacial	40	−33.10	3.558	89	84	94	24	2.84E-12				
VM30-96A	Glacial	40	−33.10	3.138	77	72	94	23	2.78E-12				
VM30-94A	Glacial	35.5	−37.80	1.238	25	23	89	18	2.20E-12	2.24E-12	3.7	543.2	14.4
VM30-94A	Glacial	35.5	−37.80	1.214	25	23	92	19	2.28E-12				
VM2616	Glacial	30.2	−45.10	0.994	25	23	92	24	2.83E-12	2.76E-12	8.7	673.6	33.0
VM26-16	Glacial	30.2	−45.10	1.112	28	24	86	22	2.59E-12				
VM26-16	Glacial	30.2	−45.10	1.893	49	43	87	22	2.71E-12				
VM26-16	Glacial	30.2	−45.10	1.756	49	42	87	24	2.90E-12				
VM26-17	Glacial	29.9	−45.10	1.378	27	24	88	17	2.10E-12	2.18E-12	6.9	522.4	25.4
VM26-17	Glacial	29.9	−45.10	1.316	27	25	90	19	2.25E-12				
VM22-26(B)	Glacial	8.7	−41.30	1.290	13	11	82	8	9.87E-13	9.77E-13	2.0	264.1	3.8
VM22-26(B)	Glacial	8.7	−41.30	1.009	10	8	79	8	9.67E-13				
VM25-60	Glacial	3.3	−34.80	1.312	18	14	79	11	1.28E-12	1.31E-12	4.3	335.5	10.2
VM25–60	Glacial	3.3	−34.80	1.418	19	16	84	11	1.34E-12				
RC13-188	Glacial	1.8	−33.70	1.073	13	10	77	9	1.12E-12	1.43E-12	23.5	296.6	46.3
RC13-188	Glacial	1.8	−33.70	1.282	19	15	84	12	1.46E-12				
RC13-188	Glacial	1.8	−33.70	4.792	69	60	88	13	1.51E-12				
RC13-188	Glacial	1.8	−33.70	4.834	76	66	87	14	1.64E-12				
VM22-32	Glacial	0.9	−31.80	1.281	15	12	78	9	1.09E-12	1.18E-12	15.4	290.5	31.6
VM22-32	Glacial	0.9	−31.80	1.355	18	14	79	11	1.28E-12				
RC24-10	Glacial	−2.2	−11.30	1.324	14	5	38	4	4.96E-13	5.38E-13	15.5	137.7	15.1
RC24-10	Glacial	−2.2	−11.30	1.022	12	5	40	5	5.80E-13				
VM22-175	Glacial	−8.8	−14.30	0.800	6	4	67	5	5.79E-13	5.80E-13	0.3	159.7	0.4
VM22-175	Glacial	−8.8	−14.30	1.500	11	7	68	5	5.81E-13				
RC16-77	Glacial	−12.7	−13.40	1.053	13	7	50	6	7.51E-13	9.01E-13	7.2	204.3	33.5
RC16-77	Glacial	−12.7	−13.40	1.246	17	8	50	7	8.15E-13				
RC16-77	Glacial	−12.7	−13.40	2.179	32	20	61	9	1.08E-12				
RC16-77	Glacial	−12.7	−13.40	2.446	34	19	56	8	9.57E-13				
VM16-36A	Glacial	−19.4	−11.40	1.120	8	7	84	6	7.17E-13	7.19E-13	0.6	195.7	0.9
VM16-36A	Glacial	−19.4	−11.40	1.407	10	8	87	6	7.22E-13				
RC8-19	Glacial	−24.3	−14.70	1.328	10	7	72	6	6.71E-13	6.92E-13	6.3	183.6	8.1
RC8-19	Glacial	−24.3	−14.70	1.315	11	8	68	6	7.14E-13				
RC12-292	Glacial	−39.7	−15.50	2.525	17	10	59	4	4.83E-13	5.06E-13	8.9	134.1	8.4
RC12-292	Glacial	−39.7	−15.50	2.774	27	12	45	4	5.28E-13				

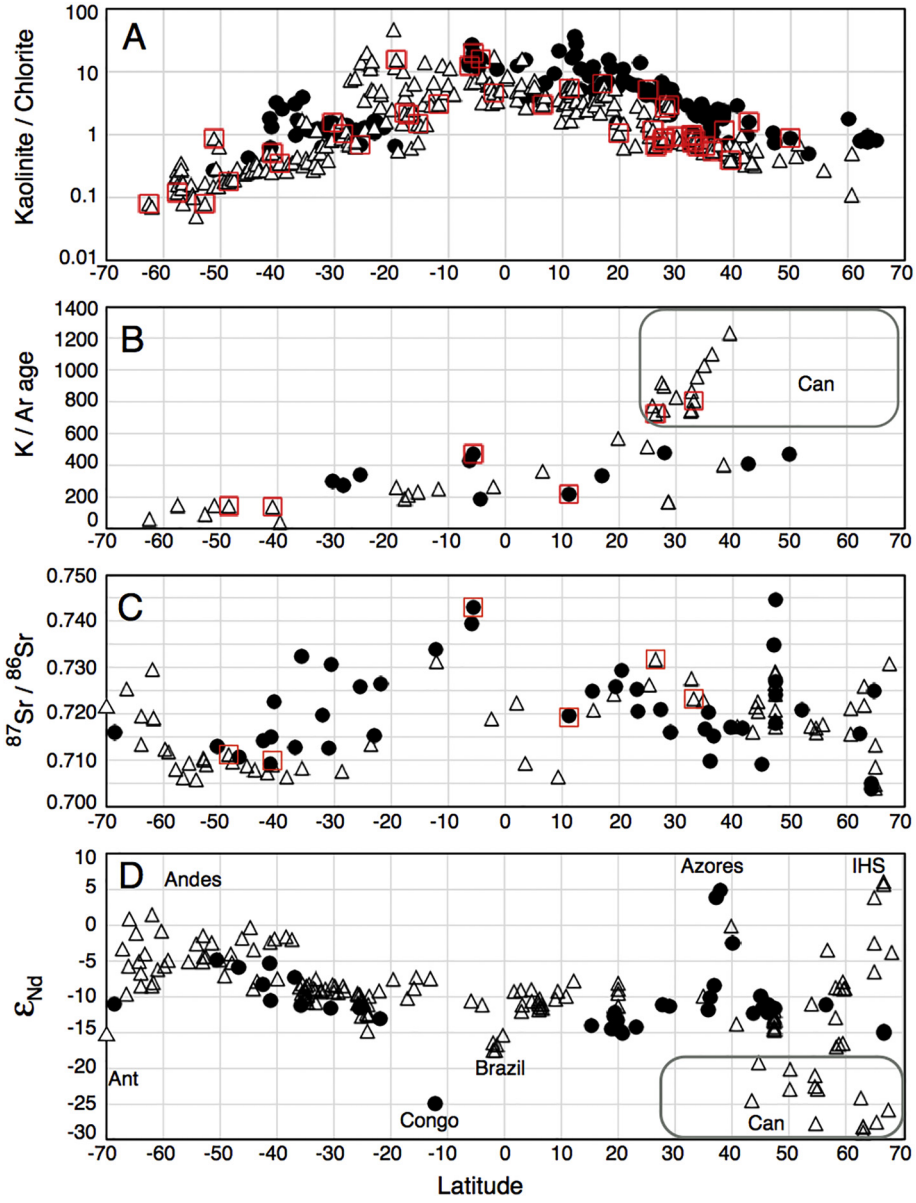

Fig. 4. Latitudinal distributions of terrigenous sediment compositions from eastern (circles) and western (triangles) basins the Atlantic Ocean. A) Kaolinite/Chlorite ratio (Biscaye, 1965). Larger squares highlight samples for which K/Ar age values have been measured. B) K/Ar age values reported in this study. Larger squares highlight samples for which $^{87}Sr/^{86}Sr$ (Dasch, 1969) are also available. C) $^{87}Sr/^{86}Sr$ from published studies. Data sources as for Fig. 3. D) ε_{Nd} from published studies. Data sources as for Fig. 3. Specific regions that stand out are labeled on the plots. Can = Canadian shield.

The trends for $^{87}Sr/^{86}Sr$ are also broadly consistent (Figs. 3, 4, 5) with higher values generally going with older K/Ar and lower ε_{Nd}, but the trends are less predictable due to the multiple processes that influence $^{87}Sr/^{86}Sr$ (importantly including grain size effects- samples from different studies have been treated differently and analyses are made on different grain sizes).

Although the ε_{Nd} data are too sparse to demonstrate it, the K/Ar ages show sources older than the adjacent North American continent off of the southern US (Fig. 3) and the clay mineralogy is less weathered in western basin sediments than in eastern basin sediments (Figs. 1, 4a) even though the surface currents would move sediments from more tropical environments to the north with the clockwise gyre. Thus it appears that the old Canadian Shield signal is transferred south by deep ocean currents such as the ones responsible for the large sediment accumulation in the Bermuda Rise (Keigwin, 2001).

As can be seen in the $^{87}Sr/^{86}Sr$ data (Fig. 4a), western basin samples south of 25°N (and not including A181–4, which is off the Amazon) also follow an increasing trend from south to north. However, north of 25°N the $^{87}Sr/^{86}Sr$ shows a strong negative trend with latitude. This strong trend highlights the significantly low values of $^{87}Sr/^{86}Sr$ in the Canadian Shield compared to European sources for a comparable ε_{Nd} (Grousset et al., 2001). Although the number of samples with both K/Ar ages and $^{87}Sr/^{86}Sr$ is small, the opposing trend of the two systems in the subpolar North Atlantic is clear (Fig. 5b) and the combination of these tracers could provide added precision in studies of North Atlantic ice rafting.

4.2. The Holocene-LGM comparison along the MAR

The MAR Holocene data are shown with east and west Atlantic basin data in Fig. 6a and Holocene and LGM data are shown in plots against latitude in Fig. 6b. Holocene MAR samples follow a trend between those of western and eastern basin compositions, except between 2° and 9°S where age values appear to be younger than found in either

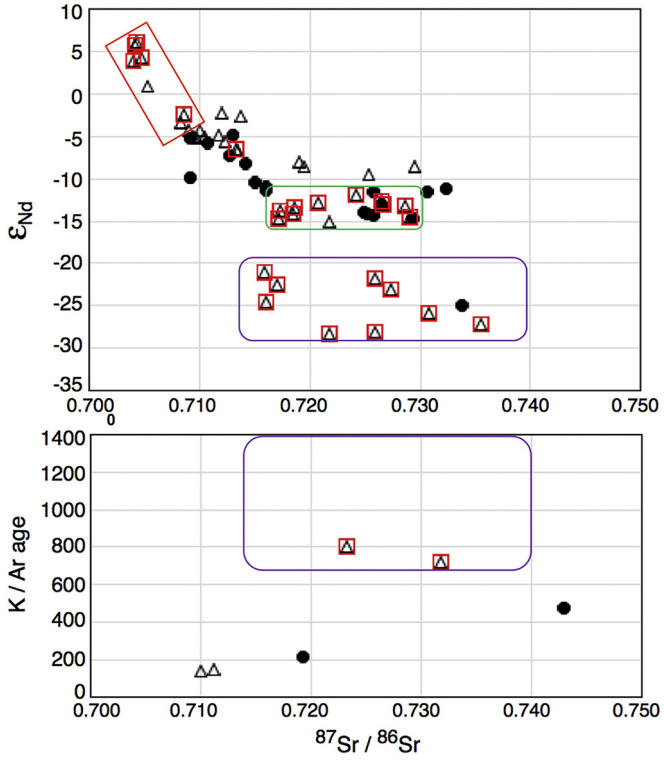

Fig. 5. Cross plots of $^{87}Sr/^{86}Sr$ against ε_{Nd} (A) and K/Ar (B) for Atlantic surface sediment samples from the eastern (circles) and western (squares) sides of the MAR where both measurements are available. Data sources as for Fig. 3. Note the reverse trend of K/Ar vs. $^{87}Sr/^{86}Sr$ for samples from west of the mid-Atlantic ridge with ancient sources. Boxes indicate specific source characteristics: red- young volcanics of the Iceland hotspot, green- Gulf of St Lawrence character, purple- ancient Canadian shield.

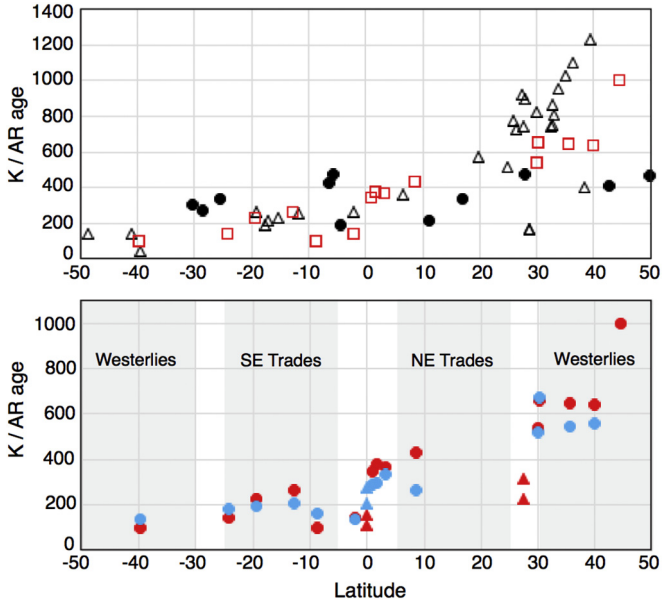

Fig. 6. Latitudinal distribution of K/Ar age values of Atlantic samples. A) Samples from eastern (circles) and western (triangles) basins as from Fig. 4, along with surface samples (larger squares) along the MAR. B) Holocene (red) and LGM (blue) samples from this study taken from cores along the MAR. Also shown are published data (warm = red triangles, cold = blue triangles) (Hurley et al., 1963a) from sites at 0.05 N, 24.17 W and 27.30 N, 34.12 W. The approximate latitudes of the trade winds and westerlies are shown along the bottom.

east or western basin samples from this latitude interval. The published warm interval data from the equator (Hurley et al., 1963a) extend the latitudinal range of this young provenance to 0°. This offset is intriguing, and could have implications for paleoclimate studies if it could be explained by the South Atlantic wind patterns. The ITCZ (thermal equator) was shifted to the south during the LGM, and extremely so during Heinrich events (Wang et al., 2007), and this could have led to a different distribution of sources to the MAR in the tropics. An alternative explanation to wind deposition is that the ridge itself is contributing younger material to these samples, but it would then be puzzling why all the MAR ages were not offset to younger ages. The southeast trade winds might be expected to bring sediment similar to that found in the eastern basin to the south of this latitude range. The eastern basin sample from 4.38°S is close in age, so this may be the expression of the wind-blown component from that latitude interval; however, the eastern basin samples from near 6°S are significantly older. Admittedly the coverage is sparse, and more samples would be required to resolve these questions.

The LGM samples at 2°S and 0.05–3°N have similar K/Ar ages as their Holocene counterparts (Fig. 6b), and the latitudinal trends in the South Atlantic part of the MAR appear to be muted relative to their Holocene counterparts. At 12.7°S the glacial value is lower and there appears to be a crossover to higher ages of glacial samples between there and 24.3°S. There is a sharp difference to older age values in samples deposited in cold intervals at the equator (Hurley et al., 1963a). Additionally, a significantly younger LGM K/Ar age is documented at 8.7°N. The LGM values for Hurley's equatorial site as well as from the 8.7 N site from this study are similar to surface values reported by Hurley off the Sahara, and may indicate greater contributions from the Sahara during cold times in this latitude interval. At 35.5°N and 40°N LGM K/Ar age values are younger, which is a little surprising since we night expect more detritus from Canadian Shield sources in the LGM. It could be that this signal is due to the increase in southeastern Laurentide ice sheet sources during the LGM (Appalachian and Grenville sources). However, more analyses would be needed to distinguish between lack of homogeneity in the sources of these sediments and significant changes in sediment sources between Holocene and LGM.

4.3. The K/Ar system in terrigenous sediments as a provenance tool

The data presented here from the Atlantic also support the promise of K/Ar in marine sediments as a tracer of terrigenous sources. The patterns of variation can be easily understood in the context of clay mineralogy, $^{87}Sr/^{86}Sr$, ε_{Nd}, combined with the geology on the surrounding continents the surface (and deep) currents and the winds. The broad scale of the sampling only hints at the applications, and for any detailed application further groundwork would be required. However, it appears that there may be shifts in the composition of terrigenous supply between Holocene and LGM at some locations along the MAR that highlight the potential for using this approach to examine changes in the boundaries between the easterly and westerly winds, intensification of winds, changes in the position of the ITCZ, changes in the trajectory of the North Atlantic current and potentially in iceberg and/or meltwater sources. It would be desirable to have greater resolution along the African margin in the latitude range of the Sahara as it appears that there is significant provenance change during the Holocene African humid period (Cole et al., 2009). It is expected that the distinctive signal from Canadian Shield sources in the northwestern basin may point to potential for understanding sediment transport to the south, to the Bermuda Rise. The clear difference between eastern and western sources in the North Atlantic and the opposing variation of $^{87}Sr/^{86}Sr$ suggest interesting applications for following iceberg tracks from the northern hemisphere glaciers. The strong gradient in compositions along the South American margin suggest the potential of using sediment provenance to track changes in the depths of North Atlantic Deep water- flowing south along the margin and carrying sediment

from older sources relative to Antarctic Intermediate and Deep Waters-flowing north along the margin and carrying sediment from younger sources (e.g., Curry and Oppo, 2005). Evidence for dispersal of sediment along the boundary current in Greenland (Innocent et al., 2000) demonstrates the source signal can be transmitted by fine sediments carried in bottom currents.

The map patterns of $^{87}Sr/^{86}Sr$ and ε_{Nd} provide a good framework for considering the K/Ar age results (Fig. 3), and I provide a review of compiled published data in the following.

4.4. Sr and Nd isotopes in Atlantic marine sediments

As demonstrated by early work (Goldstein and Jacobsen, 1988; Goldstein et al., 1984; McCulloch and Wasserburg, 1978; Onions et al., 1983; Taylor and McLennan, 1985) and many more since, the Sm/Nd system in terrigenous sedimentary materials is a robust proxy of the average mantle extraction age of the sediments' sources, notwithstanding recent work on Himalayan rivers that has called this into question in detail (Garcon et al., 2014). Accordingly, sediment recycling may alter the mixing proportions available from the landscape, but the Sm/Nd model age of the sediment is, to a first order, unaltered. In contrast, the Rb/Sr system may be greatly altered by weathering, sorting during sediment transport, and diagenesis. Rb tends to remain with solids during weathering and diagenesis while Sr tends to be removed in solution, leading to a great enrichment in the Rb/Sr in sediments compared to their ultimate crystalline basement sources (Dasch, 1969; Goldstein, 1988; McCulloch and Wasserburg, 1978 and many more since). This also leads to a substantial grain-size effect, where finer sediments tend to have much higher Rb/Sr than their coarse-grained counterparts from the same source, and thus higher $^{87}Sr/^{86}Sr$. As a first approximation, the Rb/Sr and K/Ar systems have the same mineralogical controls wherein clays (particularly illite) have higher K and Rb concentrations and feldspars have more modest K and Rb concentrations (and low concentrations in plagioclase) and they are major hosts for Sr (especially plagioclase). Clays are also much more likely to have a sedimentary, or newly-formed soil source while feldspars are likely to have been derived from crystalline sources. The weathering breakdown of preexisting minerals releases both K and radiogenic Ar leaving the age unchanged (Hurley et al., 1963b). It is expected that there should be a good correlation between K/Ar model age and Rb/Sr model age of sediment although the assumption of initial isotope composition is less obvious for $^{87}Sr/^{86}Sr$ than for $^{40}Ar/^{36}Ar$.

There is a rich data history of $^{87}Sr/^{86}Sr$ in Atlantic Ocean sediments. Dasch (1969) made a pioneering survey of “Sr isotopes in weathering profiles, deep sea sediments and sedimentary rocks” that included 47 of the Biscaye (1965) core top samples from the Atlantic Ocean. Six of these samples overlap with the ones measured for $^{40}Ar^*$ for this study and a cross plot is shown in Fig. 5b. Biscaye and Dasch (1971) followed up with a detailed study of $^{87}Sr/^{86}Sr$ from 60 samples in the Argentine Basin as well as some sediment samples from riverine and estuarine samples from South America. Dasch (1969) and McCulloch and Wasserburg (1978) showed that sedimentary materials tends to be strongly enriched in Rb/Sr relative to continental sources, and therefore they give model ages that are significantly younger than their sources. However, for near-modern sediments, the great variability that comes from sedimentary diagenesis and metamorphic and weathering processes leads to a large range in $^{87}Sr/^{86}Sr$ that can be an advantage for tracing sediment pathways. The provenance signal is potentially very large relative to the measurement uncertainty, but it is necessary to make surveys to characterize the compositions of potential sources, and it is important to consider that the Rb/Sr ratio is very high in illite and therefore there is a strong grain-size effect on the $^{87}Sr/^{86}Sr$ of terrigenous sediments. Several studies (Cole et al., 2009; Grousset and Biscaye, 1989, 2005) used $^{87}Sr/^{86}Sr$ to examine the distribution of wind-blown particulates and their expression in Atlantic sediments. McLennan et al. (1990) made a global survey of deep-sea turbidites, including $^{87}Sr/^{86}Sr$ compositions. Several papers have used the $^{87}Sr/^{86}Sr$ compositions of sediments from the North Atlantic to examine ice-rafted detritus sources as well as sediment dispersion along drift deposits (Farmer et al., 2003; Revel et al., 1996). Walter et al. (2000) showed that sediment contributions from the Weddell Sea could be traced into the South Atlantic based on their $^{87}Sr/^{86}Sr$. Franzese et al. (2006) showed that sediment contributions from the Agulhas Current “leakage” could be traced into the South Atlantic based on their $^{87}Sr/^{86}Sr$. A compilation of the relevant $^{87}Sr/^{86}Sr$ data for the Atlantic Ocean, including data from riverine particulates (Goldstein and Jacobsen, 1988), is shown in Fig. 3b.

Following the demonstration that the Sm/Nd isotope system in sedimentary materials is not altered from that of its source (McCulloch and Wasserburg, 1978), this system has become one of the most widely used geochemical provenance tools, and with rare exceptions (Awwiller and Mack, 1991; Bock et al., 1994; Lev et al., 1999; McDaniel et al., 1994) it is a robust provenance tool in sedimentary deposits throughout Earth's history. Grousset et al. (1988) presented Sm/Nd data from surface sediments in the North Atlantic, mostly in the northeast Atlantic basin. They interpreted the distribution between 40° and 50° North to be from North American sources via the westerly winds, and between 0° and 30° North to be from Saharan sources via the trade winds, both consistent with the inference from clay mineralogy (Griffin et al., 1968). Grousset and Biscaye (2005) reviewed their findings for Nd, Sr and Pb isotopes in ocean sediments and ice cores. Many of the references cited above in the $^{87}Sr/^{86}Sr$ summary also provided ε_{Nd} data (Farmer et al., 2003; Franzese et al., 2006; Franzese et al., 2009; McLennan et al., 1990; Revel et al., 1996; Walter et al., 2000), and additional ε_{Nd} data from terrigenous sediments in the North Atlantic and Labrador Sea come from a variety of sources (Fagel et al., 2004, 1999; Fagel and Mattielli, 2011; Innocent et al., 2000, 1997; White and Dupre, 1986). A compilation of the relevant ε_{Nd} data for the Atlantic Ocean, including data from riverine particulates (Goldstein and Jacobsen, 1988; Goldstein et al., 1984), is shown in Fig. 3c.

In sedimentary rocks, the pairing of ε_{Nd} with $^{87}Sr/^{86}Sr$ is hampered by the open-system behavior of the Rb/Sr system during burial diagenesis, but in young sediments the pairing of these systems is quite powerful and widely used (Fig. 5a). To a good first approximation, as reviewed above, ε_{Nd} can be thought of as a simple monitor of average crustal extraction age. Accordingly, it is a frame of reference in which to consider the deviation of the $^{87}Sr/^{86}Sr$ from a narrow linear array, which can be understood by the greater tendency for Rb and Sr to be separated from each other during many geologic processes. Fig. 5b displays the published data from Atlantic surface sediments where both ε_{Nd} and $^{87}Sr/^{86}Sr$ are reported.

4.5. Summary of observations and future directions

The K/Ar (or Ar/Ar) age of a terrigenous sediment is a robust provenance approach, that is dominantly a signal of the concentration of ingrown radiogenic argon, $^{40}Ar^*$. The sample preparations and measurements are rapid and simple, so this is a desirable tool for tracing provenance and could provide a means of surveying a large number of samples and then selecting a subset for application of a wider range of geochemical measures. As one of the earliest widely-applied chronometers, there is substantial archived data from crystalline source terrains. However, because of the significant alteration of the signal in recycled sedimentary rocks, and the great fraction of recycled sedimentary rocks in sediments, it is necessary to establish appropriate regional trends as background information for specific applications. The K/Ar ages of clays in Atlantic Ocean follow systematic trends that broadly reflect the geology of their source areas and the path they took to their final deposition. The pattern of K/Ar ages complements those from clay mineralogy $^{87}Sr/^{86}Sr$ and ε_{Nd}. Although the major elements were not measured for this study, the acquisition of K concentrations and other major elements would also allow making inferences about the

weathering of the sediments' sources.

Declarations of interests

None.

Acknowledgements

The sample processing and data collection were aided by Byrdie Renik as a post-baccalaureate research assistant at LDEO funded by a GSA Easterbrook award to Wally Broecker. Pierre Biscaye is thanked for providing the clay fractions from his study of clay mineralogy in the Atlantic. A grant from the Lamont Climate Center funded some of the analyses. Special thanks go to Christine Kassab for her help with creating the maps. Thanks to Karen Benedetto for scanning the Biscaye thesis, to Merry Cai and her interns for “rescuing” the Biscaye data and making them available digitally, and to Patty Catanzaro and Katie Wooton for help with drafting. Thanks also for the efforts of editor Gert J. De Lange as well as reviews from Nathalie Fagel and an anonymous reviewer.

References

Aarons, S.M., Aciego, S.M., Gleason, J.D., 2013. Variable Hf-Sr-Nd radiogenic isotopic compositions in a Saharan dust storm over the Atlantic: Implications for dust flux to oceans, ice sheets and the terrestrial biosphere. Chem. Geol. 349, 18–26. https://doi.org/10.1016/j.chemgeo.2013.04.010.

Aronson, J.L., Hower, J., 1976. Mechanism of burial metamorphism of argillaceous sediment: 2. Radiogenic argon evidence. Bull. Geol. Soc. Am. https://doi.org/10.1130/0016-7606(1976)87<738:MOBMOA>2.0.CO;2.

Awwiller, D.N., Mack, L.E., 1991. Diagenetic modification of SM-ND model ages in tertiary sandstones and shales, Texas gulf-coast. Geology 19, 311–314. https://doi.org/10.1130/0091-7613(1991)019<0311:dmosnm>2.3.co;2.

Basile, I., Grousset, F.E., Revel, M., Petit, J.R., Biscaye, P.E., Barkov, N.I., 1997. Patagonian origin of glacial dust deposited in East Antarctica (Vostok and Dome C) during glacial stages 2, 4 and 6. Earth Planet. Sci. Lett. 146, 573–589. https://doi.org/10.1016/s0012-821x(96)00255-5.

Biscaye, P.E., 1965. Mineralogy and sedimentation of recent deep-sea clay in Atlantic Ocean and adjacent seas and oceans. Geol. Soc. Am. Bull. 76https://doi.org/10.1130/0016-7606(1965)76[803:masord]2.0.co;2. (803-).

Biscaye, P.E., Dasch, E.J., 1971. Rubidium, strontium, strontium-isotope system in deep-sea sediments - Argentine basin. J. Geophys. Res. 76https://doi.org/10.1029/JC076i021p05087. (5087-).

Bock, B., McLennan, S.M., Hanson, G.N., 1994. Rare-earth element redistribution and its effects on the neodymium isotope system in the Austin-Glen member of the Normanskill formation, New-York, USA. Geochim. Cosmochim. Acta 58, 5245–5253. https://doi.org/10.1016/0016-7037(94)90308-5.

Bond, G., Heinrich, H., Broecker, W., Labeyrie, L., McManus, J., Andrews, J., Huon, S., Jantschik, R., Clasen, S., Simet, C., Tedesco, K., Klas, M., Bonani, G., Ivy, S., 1992. Evidence for massive discharges of icebergs into the North-Atlantic Ocean during the last glacial period. Nature 360, 245–249. https://doi.org/10.1038/360245a0.

Broecker, W., Bond, G., Klas, M., Clark, E., McManus, J., 1992. Origin of the northern Atlantic's Heinrich events. Clim. Dyn. 6, 265–273. https://doi.org/10.1007/bf00193540.

Chester, R., Hughes, M.J., 1969. Trace element geochemistry of a north pacific pelagic clay core. Deep. Res. 16https://doi.org/10.1016/0011-7471(69)90064-3. (639-).

Clauer, N., Chaudhuri, S., 1995. Clays in Crustal Environments: Isotope Dating and Tracing. https://doi.org/10.1007/978-3-642-79085-0.

Cole, J.M., Goldstein, S.L., deMenocal, P.B., Hemming, S.R., Grousset, F.E., 2009. Contrasting compositions of Saharan dust in the eastern Atlantic Ocean during the last deglaciation and African Humid Period. Earth Planet. Sci. Lett. 278. https://doi.org/10.1016/j.epsl.2008.12.011.

Cook, C.P., Hemming, S.R., van de Flierdt, T., Pierce Davis, E.L., Williams, T., Galindo, A.L., Jiménez-Espejo, F.J., Escutia, C., 2017. Glacial erosion of east Antarctica in the Pliocene: a comparative study of multiple marine sediment provenance tracers. Chem. Geol. 466. https://doi.org/10.1016/j.chemgeo.2017.06.011.

Curry, W.B., Oppo, D.W., 2005. Glacial water mass geometry and the distribution of delta C-13 of Sigma CO2 in the western Atlantic Ocean. Paleoceanography 20. https://doi.org/10.1029/2004pa001021.

Dasch, E.J., 1969. Strontium isotopes in weathering profiles, deep-sea sediments, and sedimentary rocks. Geochim. Cosmochim. Acta 33https://doi.org/10.1016/0016-7037(69)90153-7. (1521-).

de Mahiques, M.M., Tassinari, C.C.G., Marcolini, S., Violante, R.A., Figueira, R.C.L., da Silveira, I.C.A., Burone, L., Sousa, S.H.D., 2008. Nd and Pb isotope signatures on the southeastern South American upper margin: implications for sediment transport and source rocks. Mar. Geol. 250, 51–63. https://doi.org/10.1016/j.margeo.2007.11.007.

DePaolo, D.J., Maher, K., Christensen, J.N., McManus, J., 2006. Sediment transport time measured with U-series isotopes: results from ODP North Atlantic drift site 984. Earth Planet. Sci. Lett. 248, 394–410. https://doi.org/10.1016/j.epsl.2006.06.004.

Derkowski, A., Srodon, J., Franus, W., Uhlik, P., Banas, M., Zielinski, G., Caplovicova, M., Franus, M., 2009. Partial dissolution of glauconitic samples: implications for the methodology of K-Ar and Rb-Sr dating. Clay Clay Miner. 57, 531–554. https://doi.org/10.1346/ccmn.2009.0570503.

Fagel, N., Mattielli, N., 2011. Holocene evolution of deep circulation in the northern North Atlantic traced by Sm, Nd and Pb isotopes and bulk sediment mineralogy. Paleoceanography 26, 15. https://doi.org/10.1029/2011pa002168.

Fagel, N., Innocent, C., Stevenson, R.K., Hillaire-Marcel, C., 1999. Deep circulation changes in the Labrador sea since the last glacial maximum: new constraints from Sm-Nd data on sediments. Paleoceanography 14, 777–788. https://doi.org/10.1029/1999pa900041.

Fagel, N., Hillaire-Marcel, C., Humblet, M., Brasseur, R., Weis, D., Stevenson, R., 2004. Nd and Pb isotope signatures of the clay-size fraction of Labrador Sea sediments during the Holocene: implications for the inception of the modern deep circulation pattern. Paleoceanography 19, 16. https://doi.org/10.1029/2003pa000993.

Farmer, G.L., Barber, D., Andrews, J., 2003. Provenance of Late Quaternary ice-proximal sediments in the North Atlantic: Nd, Sr and Pb isotopic evidence. Earth Planet. Sci. Lett. 209, 227–243. https://doi.org/10.1016/s0012-821x(03)00068-2.

Franzese, A.M., Hemming, S.R., 2013. Terrigenous Sediments, Encyclopedia of Quaternary Science, Second edition. https://doi.org/10.1016/B978-0-444-53643-3.00296-X.

Franzese, A.M., Hemming, S.R., Goldstein, S.L., Anderson, R.F., 2006. Reduced Agulhas leakage during the Last Glacial Maximum inferred from an integrated provenance and flux study. Earth Planet. Sci. Lett. 250. https://doi.org/10.1016/j.epsl.2006.07.002.

Franzese, A.M., Hemming, S.R., Goldstein, S.L., 2009. Use of strontium isotopes in detrital sediments to constrain the glacial position of the Agulhas Retroflection. Paleoceanography 24, 12. https://doi.org/10.1029/2008pa001706.

Garcon, M., Chauvel, C., France-Lanord, C., Limonta, M., Garzanti, E., 2014. Which minerals control the Nd-Hf-Sr-Pb isotopic compositions of river sediments? Chem. Geol. 364, 42–55. https://doi.org/10.1016/j.chemgeo.2013.11.018.

Garzanti, E., Ando, S., Vezzoli, G., 2009. Grain-size dependence of sediment composition and environmental bias in provenance studies. Earth Planet. Sci. Lett. 277, 422–432. https://doi.org/10.1016/j.epsl.2008.11.007.

Gehrels, G., 2014. Detrital zircon U-Pb geochronology applied to tectonics. In: Jeanloz, R. (Ed.), Annual Review of Earth and Planetary Sciences. Vol 42. Annual Reviews, Palo Alto, pp. 127–149. https://doi.org/10.1146/annurev-earth-050212-124012.

Goldich, S.S., 1938. A study in rock-weathering. J. Geol. 46, 17–58. https://doi.org/10.1086/624619.

Goldstein, S.L., 1988. Decoupled evolution of Nd and Sr isotopes in the continental-crust and the mantle. Nature 336, 733–738. https://doi.org/10.1038/336733a0.

Goldstein, S.J., Jacobsen, S.B., 1988. Nd and Sr isotopic systematics of river water suspended material - implications for crustal evolution. Earth Planet. Sci. Lett. 87, 249–265. https://doi.org/10.1016/0012-821x(88)90013-1.

Goldstein, S.L., Onions, R.K., Hamilton, P.J., 1984. A Sm-Nd isotopic study of atmospheric dusts and particulates from major river systems. Earth Planet. Sci. Lett. 70, 221–236. https://doi.org/10.1016/0012-821x(84)90007-4.

Gombiner, J.H., Hemming, S.R., Hendy, I.L., Bryce, J.G., Blichert-Toft, J., 2016. Isotopic and elemental evidence for Scabland Flood sediments offshore Vancouver Island. Quat. Sci. Rev. 139. https://doi.org/10.1016/j.quascirev.2016.02.026.

Griffin, J.J., Windom, H., Goldberg, E.D., 1968. Distribution of clay minerals in world ocean. Deep. Res. 15https://doi.org/10.1016/0011-7471(68)90051-x. (433-).

Grousset, F.E., Biscaye, P.E., 1989. Nd And Sr isotopes as tracers of wind transport - Atlantic aerosols and surface sediments. In: Paleoclimatology and Paleometeorology: Modern and Past Patterns of Global Atmospheric Transport. Kluwer Academic Publ, Dordrecht.

Grousset, F.E., Biscaye, P.E., 2005. Tracing dust sources and transport patterns using Sr, Nd and Pb isotopes. Chem. Geol. 222, 149–167. https://doi.org/10.1016/j.chemgeo.2005.05.006.

Grousset, F.E., Biscaye, P.E., Zindler, A., Prospero, J., Chester, R., 1988. Neodymium isotopes as tracers in marine-sediments and aerosols - North-Atlantic. Earth Planet. Sci. Lett. 87, 367–378. https://doi.org/10.1016/0012-821x(88)90001-5.

Grousset, F.E., Labeyrie, L., Sinko, J.A., Cremer, M., Bond, G., Duprat, J., Cortijo, E., Huon, S., 1993. Patterns of ice-rafted detritus in the glacial North-Atlantic (40-degrees-55-degrees-N). Paleoceanography 8, 175–192. https://doi.org/10.1029/92pa02923.

Grousset, F.E., Parra, M., Bory, A., Martinez, P., Bertrand, P., Shimmield, G., Ellam, R.M., 1998. Saharan wind regimes traced by the Sr-Nd isotopic composition of subtropical Atlantic sediments: Last Glacial maximum vs today. Quat. Sci. Rev. 17, 395–409. https://doi.org/10.1016/s0277-3791(97)00048-6.

Grousset, F.E., Cortijo, E., Huon, S., Herve, L., Richter, T., Burdloff, D., Duprat, J., Weber, O., 2001. Zooming in on Heinrich layers. Paleoceanography 16, 240–259. https://doi.org/10.1029/2000pa000559.

Hegner, E., Daulelsberg, H.J., van der Loeff, M.M.R., Jeandel, C., de Baar, H.J.W., 2007. Nd isotopic constraints on the origin of suspended particles in the Atlantic sector of the Southern Ocean. Geochem. Geophys. Geosyst. 8, 18. https://doi.org/10.1029/2007gc001666.

Heinrich, H., 1988. Origin and consequences of cyclic ice rafting in the northeast Atlantic-Ocean during the past 130,000 years. Quat. Res. 29, 142–152. https://doi.org/10.1016/0033-5894(88)90057-9.

Hemming, S.R., 2004. Heinrich events: massive late pleistocene detritus layers of the North Atlantic and their global climate imprint. Rev. Geophys. 42, 43. https://doi.org/10.1029/2003rg000128.

Hemming, S.R., Hall, C.M., Biscaye, P.E., Higgins, S.M., Bond, G.C., McManus, J.F., Barber, D.C., Andrews, J.T., Broecker, W.S., 2002. $^{40}Ar/^{39}Ar$ ages and $^{40}Ar^{*}$ concentrations of fine-grained sediment fractions from North Atlantic Heinrich layers. Chem. Geol. 182. https://doi.org/10.1016/S0009-2541(01)00342-4.

Huon, S., Jantschik, R., 1993. Detrital silicates in northeast Atlantic deep-sea sediments during the Late Quaternary - major-element, REE and Rb-Sr Isotopic data. Eclogae Geol. Helv. 86, 195–218.

Huon, S., Ruch, P., 1992. Mineralogical, K-Ar and Sr-87/Sr-86 isotope studies of Holocene and Late Glacial sediments in a deep-sea core from the northeast Atlantic-Ocean. Mar.

Geol. 107, 275–282. https://doi.org/10.1016/0025-3227(92)90076-t.
Hurbert, J.F., 1962. A zircon-tourmaline-rutile maturity index and the interdependence of the composition of heavy mineral assemblages with the gross composition and texture of sandstones. J. Sediment. Res. 32, 440–450. https://doi.org/10.1306/74D70CE5-2B21-11D7-8648000102C1865D.
Hurley, P.M., 1961. Glauconite as a possible means of measuring age of sediments. Ann. N. Y. Acad. Sci. 91https://doi.org/10.1111/j.1749-6632.1961.tb35463.x. (294-).
Hurley, P.M., Brookins, D.G., Pinson, W.H., Hart, S.R., Fairbairn, H.W., 1961. K-Ar age studies of mississippi and other river sediments. Geol. Soc. Am. Bull. 72, 1807–1816. https://doi.org/10.1130/0016-7606(1961)72[1807:kasoma]2.0.co;2.
Hurley, P.M., Heezen, B.C., Pinson, W.H., Fairbairn, H.W., 1963a. K-Ar age values in pelagic sediments of the North-Atlantic. Geochim. Cosmochim. Acta 27, 393–399. https://doi.org/10.1016/0016-7037(63)90078-4.
Hurley, P.M., Hunt, J.M., Pinson, W.H., Fairbairn, H.W., 1963b. K-Ar age values on the clay fractions in dated shales. Geochim. Cosmochim. Acta 27, 279–284. https://doi.org/10.1016/0016-7037(63)90031-0.
Innocent, C., Fagel, N., Stevenson, R.K., HillaireMarcel, C., 1997. Sm-Nd signature of modern and late Quaternary sediments from the northwest North Atlantic: Implications for deep current changes since the Last Glacial Maximum. Earth Planet. Sci. Lett. 146, 607–625. https://doi.org/10.1016/s0012-821x(96)00251-8.
Innocent, C., Fagel, N., Hillaire-Marcel, C., 2000. Sm-Nd isotope systematics in deep-sea sediments: clay-size versus coarser fractions. Mar. Geol. 168, 79–87. https://doi.org/10.1016/s0025-3227(00)00052-9.
Jantschik, R., Huon, S., 1992. Detrital silicates in northeast Atlantic deep-sea sediments during the Late Quaternary - mineralogical and K-Ar isotopic data. Eclogae Geol. Helv. 85, 195–212.
Jones, C.E., Halliday, A.N., Rea, D.K., Owen, R.M., 1994. Neodymium isotopic variations in North Pacific modern silicate sediment and the insignificance of detrital REE contributions to seawater. Earth Planet. Sci. Lett. 127, 55–66. https://doi.org/10.1016/0012-821x(94)90197-x.
Keigwin, L.D., 2001. Data report: late Pleistocene stable isotope studies of ODP Sites 1054, 1055, and 1063. In: Proc. ODP Sci. Results.
Kumar, A., Abouchami, W., Galer, S.J.G., Garrison, V.H., Williams, E., Andreae, M.O., 2014. A radiogenic isotope tracer study of transatlantic dust transport from Africa to the Caribbean. Atmos. Environ. 82, 130–143. https://doi.org/10.1016/j.atmosenv.2013.10.021.
Lev, S.M., McLennan, S.M., Hanson, G.N., 1999. Mineralogic controls on REE mobility during black-shale diagenesis. J. Sediment. Res. 69, 1071–1082. https://doi.org/10.2110/jsr.69.1071.
Licht, K.J., Hemming, S.R., 2017. Analysis of Antarctic glacigenic sediment provenance through geochemical and petrologic applications. Quat. Sci. Rev. 164. https://doi.org/10.1016/j.quascirev.2017.03.009.
McCulloch, M.T., Wasserburg, G.J., 1978. Sm-Nd AND Rb-Sr chronology of continental crust formation. Science 200, 1003–1011. https://doi.org/10.1126/science.200.4345.1003. 80-.
McDaniel, D.K., Hemming, S.R., McLennan, S.M., Hanson, G.N., 1994. Resetting of neodymium isotopes and redistribution of REEs during sedimentary processes - the Early Proterozoic Chelmsford formation, Sudbury Basin, Ontario, Canada. Geochim. Cosmochim. Acta 58, 931–941. https://doi.org/10.1016/0016-7037(94)90516-9.
McLennan, S.M., 1993. Weathering and global denudation. J. Geol. 101, 295–303. https://doi.org/10.1086/648222.
McLennan, S.M., Taylor, S.R., McCulloch, M.T., Maynard, J.B., 1990. Geochemical and Nd-Sr isotopic composition of deep-sea turbidites - crustal evolution and plate tectonic associations. Geochim. Cosmochim. Acta 54, 2015–2050. https://doi.org/10.1016/0016-7037(90)90269-q.
McManus, J.F., Anderson, R.F., Broecker, W.S., Fleisher, M.Q., Higgins, S.M., 1998. Radiometrically determined sedimentary fluxes in the sub-polar North Atlantic during the last 140,000 years. Earth Planet. Sci. Lett. 155, 29–43. https://doi.org/10.1016/s0012-821x(97)00201-x.
Meyer, I., Davies, G.R., Stuut, J.B.W., 2011. Grain size control on Sr-Nd isotope provenance studies and impact on paleoclimate reconstructions: an example from deep-sea sediments offshore NW Africa. Geochem. Geophys. Geosyst. 12, 14. https://doi.org/10.1029/2010gc003355.
Mezger, K., Krogstad, E.J., 1997. Interpretation of discordant U-Pb zircon ages: an evaluation. J. Metamorph. Geol. 15, 127–140. https://doi.org/10.1111/j.1525-1314.1997.00008.x.
Milliman, J.D., Meade, R.H., 1983. World-wide delivery of river sediment to the oceans. J. Geol. 91, 1–21. https://doi.org/10.1086/628741.
Milliman, J.D., Syvitski, J.P.M., 1992. Geomorphic tectonic control of sediment discharge to the ocean - the importance of small mountainous rivers. J. Geol. 100, 525–544. https://doi.org/10.1086/629606.
Moecher, D.P., Samson, S.D., 2006. Differential zircon fertility of source terranes and natural bias in the detrital zircon record: implications for sedimentary provenance analysis. Earth Planet. Sci. Lett. 247, 252–266. https://doi.org/10.1016/j.epsl.2006.04.035.
Nakai, S., Halliday, A.N., Rea, D.K., 1993. Provenance of dust in the Pacific-Ocean. Earth Planet. Sci. Lett. 119, 143–157. https://doi.org/10.1016/0012-821x(93)90012-x.
Nesbitt, H.W., Young, G.M., 1984. Prediction of some weathering trends of plutonic and volcanic-rocks based on thermodynamic and kinetic considerations. Geochim. Cosmochim. Acta 48, 1523–1534. https://doi.org/10.1016/0016-7037(84)90408-3.
Noble, T.L., Piotrowski, A.M., Robinson, L.F., McManus, J.F., Hillenbrand, C.D., Bory, A.J.M., 2012. Greater supply of Patagonian-sourced detritus and transport by the ACC to the Atlantic sector of the Southern Ocean during the last glacial period. Earth Planet. Sci. Lett. 317, 374–385. https://doi.org/10.1016/j.epsl.2011.10.007.
Odin, G.S., 1976. Galuconite GL-O, interlaboratory standard for radiochronometric analysis. Analusis 4, 287–291.
Onions, R.K., Hamilton, P.J., Hooker, P.J., 1983. A Nd isotope investigation of sediments related to crustal development in the British-isles. Earth Planet. Sci. Lett. 63, 229–240. https://doi.org/10.1016/0012-821x(83)90039-0.
Peel, M.C., Finlayson, B.L., McMahon, T.A., 2007. Updated world map of the Koppen-Geiger climate classification. Hydrol. Earth Syst. Sci. 11, 1633–1644. https://doi.org/10.5194/hess-11-1633-2007.
Petschick, R., Kuhn, G., Gingele, F., 1996. Clay mineral distribution in surface sediments of the South Atlantic: sources, transport, and relation to oceanography. Mar. Geol. 130, 203–229. https://doi.org/10.1016/0025-3227(95)00148-4.
Pettke, T., Halliday, A.N., Hall, C.M., Rea, D.K., 2000. Dust production and deposition in Asia and the North Pacific Ocean over the past 12 Myr. Earth Planet. Sci. Lett. 178, 397–413. https://doi.org/10.1016/s0012-821x(00)00083-2.
Rea, D.K., Leinen, M., Janecek, T.R., 1985. Geologic approach to the long-term history of atmospheric circulation. Science 227, 721–725. https://doi.org/10.1126/science.227.4688.721. 80-.
Reiners, P.W., Campbell, I.H., Nicolescu, S., Allen, C.M., Hourigan, J.K., Garver, J.I., Mattinson, J.M., Cowan, D.S., 2005a. (U-Th)/(HE-Pb) double dating of detrital zircons. Am. J. Sci. 305, 259–311. https://doi.org/10.2475/ajs.305.4.259.
Reiners, P.W., Ehlers, T.A., Zeitler, P.K., 2005b. Past, present, and future of thermochronology. In: Reiners, P.W., Ehlers, T.A. (Eds.), Low-temperature Thermochronology: Techniques, Interpretations, and Applications. Mineralogical Soc Amer, Chantilly, pp. 1–18. https://doi.org/10.2138/rmg.2005.58.1.
Revel, M., Sinko, J.A., Grousset, F.E., Biscaye, P.E., 1996. Sr and Nd isotopes as tracers of North Atlantic lithic particles: Paleoclimatic implications. Paleoceanography 11, 95–113. https://doi.org/10.1029/95pa03199.
Reyes, A.V., Carlson, A.E., Beard, B.L., Hatfield, R.G., Stoner, J.S., Winsor, K., Welke, B., Ullman, D.J., 2014. South Greenland ice-sheet collapse during marine isotope stage 11. Nature 510https://doi.org/10.1038/nature13456. (525–+).
Ruddiman, W.F., 1977. Late Quaternary deposition of ice-rafted sand in subpolar North-Atlantic (Lat 40-degrees to 65-degrees-N). Geol. Soc. Am. Bull. 88, 1813–1827. https://doi.org/10.1130/0016-7606(1977)88<1813:lqdois>2.0.co;2.
Rutberg, R.L., Hemming, S.R., Goldstein, S.L., 2000. Reduced orth Atlantic deep water flux to the glacial southern ocean inferred from neodymium isotope ratios. Nature 405, 935–938.
Skonieczny, C., Bory, A., Bout-Roumazeilles, V., Abouchami, W., Galer, S.J.G., Crosta, X., Diallo, A., Ndiaye, T., 2013. A three-year time series of mineral dust deposits on the West African margin: Sedimentological and geochemical signatures and implications for interpretation of marine paleo-dust records. Earth Planet. Sci. Lett. 364, 145–156. https://doi.org/10.1016/j.epsl.2012.12.039.
Steiger, R.H., Jager, E., 1977. Subcommission on geochronology - convention on use of decay constants in geochronology and cosmochronology. Earth Planet. Sci. Lett. 36, 359–362. https://doi.org/10.1016/0012-821x(77)90060-7.
Taylor, S.R., McLennan, S.M., 1985. The Continental Crust: Its Evolution and Composition. Lon Blackwell.
Thiry, M., 2000. Palaeoclimatic interpretation of clay minerals in marine deposits: an outlook from the continental origin. Earth Sci. Rev. 49, 201–221. https://doi.org/10.1016/s0012-8252(99)00054-9.
Tochilin, C.J., Reiners, P.W., Thomson, S.N., Gehrels, G.E., Hemming, S.R., Pierce, E.L., 2012. Erosional history of the Prydz Bay sector of East Antarctica from detrital apatite and zircon geo- and thermochronology multidating. Geochem. Geophys. Geosyst. 13. https://doi.org/10.1029/2012gc004364.
Toucanne, S., Soulet, G., Freslon, N., Jacinto, R.S., Dennielou, B., Zaragosi, S., Eynaud, F., Bourillet, J.F., Bayon, G., 2015. Millennial-scale fluctuations of the European Ice Sheet at the end of the last glacial, and their potential impact on global climate. Quat. Sci. Rev. 123, 113–133. https://doi.org/10.1016/j.quascirev.2015.06.010.
VanLaningham, S., Mark, D.F., 2011. Step heating of Ar-40/Ar-39 standard mineral mixtures: Investigation of a fine-grained bulk sediment provenance tool. Geochim. Cosmochim. Acta 75, 2324–2335. https://doi.org/10.1016/j.gca.2011.01.038.
VanLaningham, S., Duncan, R.A., Pisias, N.G., 2006. Erosion by rivers and transport pathways in the ocean: a provenance tool using Ar-40-Ar-39 incremental heating on fine-grained sediment. J. Geophys. Res. Surf. 111, 22. https://doi.org/10.1029/2006jf000583.
VanLaningham, S., Duncan, R.A., Pisias, N.G., Graham, D.W., 2008. Tracking fluvial response to climate change in, the Pacific Northwest: a combined provenance approach using Ar and Nd isotopic systems on fine-grained sediments. Quat. Sci. Rev. 27, 497–517. https://doi.org/10.1016/j.quascirev.2007.10.018.
VanLaningham, S., Pisias, N.G., Duncan, R.A., Clift, P.D., 2009. Glacial-interglacial sediment transport to the Meiji Drift, Northwest Pacific Ocean: evidence for timing of Beringian outwashing. Earth Planet. Sci. Lett. 277, 64–72. https://doi.org/10.1016/j.epsl.2008.09.033.
Walter, H.J., Hegner, E., Diekmann, B., Kuhn, G., van der Loeff, M.M.R., 2000. Provenance and transport of terrigenous sediment in the South Atlantic Ocean and their relations to glacial and interglacial cycles: Nd and Sr isotopic evidence. Geochim. Cosmochim. Acta 64, 3813–3827. https://doi.org/10.1016/s0016-7037(00)00476-2.
Wang, X.F., Auler, A.S., Edwards, R.L., Cheng, H., Ito, E., Wang, Y.J., Kong, X.G., Solheid, M., 2007. Millennial-scale precipitation changes in southern Brazil over the past 90,000 years. Geophys. Res. Lett. 34, 5. https://doi.org/10.1029/2007gl031149.
White, W.M., Dupre, B., 1986. Sediment subduction and magma genesis in the Lesser Antilles - isotopic and trace-element constraints. J. Geophys. Res. Earth Planets 91, 5927–5941. https://doi.org/10.1029/JB091iB06p05927.
Zhang, Y.C., Chiessi, C.M., Mulitza, S., Zabel, M., Trindade, R.I.F., Hollanda, M., Dantas, E.L., Govin, A., Tiedemann, R., Wefer, G., 2015. Origin of increased terrigenous supply to the NE South American continental margin during Heinrich Stadial 1 and the Younger Dryas. Earth Planet. Sci. Lett. 432, 493–500. https://doi.org/10.1016/j.epsl.2015.09.054.